Negative cell cycle regulation by Calcineurin is necessary for proper beta cell regeneration in zebrafish

Laura Massoz[1*], David Bergemann[1], Arnaud Lavergne[1,2], Célia Reynders[1], Caroline Désiront[1], Chiara Goossens[1], Lydie Flasse[1], Bernard Peers[1], Marianne L. Voz[1] and Isabelle Manfroid[1]

Author Affiliations

[1]Zebrafish Development and Disease Models laboratory, GIGA-Stem Cells, University of Liège, Liège, Belgium

[2]GIGA-Genomics core facility, GIGA, University of Liège, Liège, Belgium

*Corresponding author:

Email address: laura.massoz@doct.uliege.be

Abstract

Stimulation of pancreatic beta cell regeneration could be a therapeutic lead to treat diabetes. Unlike humans, the zebrafish can efficiently regenerate beta cells, notably from ductal pancreatic progenitors. To gain insight into the molecular pathways involved in this process, we established the transcriptomic profile of the ductal cells after beta cell ablation in the adult zebrafish. These data highlighted the protein phosphatase calcineurin as a new potential modulator of beta cell regeneration. We showed that calcineurin overexpression abolished the regenerative response, leading to glycemia dysregulation. On the opposite, calcineurin inhibition increased ductal cell proliferation and subsequent beta cell regeneration. Interestingly, the enhanced proliferation of the progenitors was paradoxically coupled with their exhaustion. This suggests that the proliferating progenitors are next entering in differentiation. Calcineurin appears as a guardian which prevents an excessive progenitor proliferation to preserve the pool of progenitors. Altogether, our findings reveal calcineurin as a key player in the balance between proliferation and differentiation to enable a proper beta cell regeneration.

Introduction

Blood glucose homeostasis is tightly controlled by pancreatic endocrine cells. Insulin-producing beta cells work in close association with alpha cells, which secrete glucagon, and delta cells secreting somatostatin, to maintain normal glycemia. The insulin plays a critical role in this process as it is the only hormone able to lower the glycemia. Beta cell loss is a hallmark of type 1 and of late stages of type 2 diabetes, leading to chronic hyperglycemia. Beta cell destruction is largely irreversible in human and in mammals, making the disease incurable nowadays. Nevertheless, studies in diabetic mice models uncovered promising evidences of slight recovery of beta cells via regeneration. For example, new beta cells can arise from the replication of remaining beta cells [1]. Different models of pancreas injuries revealed the plasticity of mammalian pancreatic cells. Actually, differentiated endocrine cells such as alpha cells[2] and delta cells[3] can reprogram and convert into insulin-producing cells, a process that is age dependent. Another possible source of beta cells could be de *novo* formation from pancreatic progenitors residing in the ductal compartment of the adult pancreas [4]. Lineage tracing experiments could not clearly highlight new beta cells arising from the ductal cells in the adult [4]–[6]. However, expression of the pro-endocrine marker Neurog3 was detected in the ducts in different mouse models of pancreas regeneration [4], [7], [8]. In addition, a rare population of ductal cells expressing Neurog3 has been reported to contribute to beta cell neogenesis during diabetes [9]. A recent study of single cell RNA sequencing reveal a sub-population of human ductal cells which are

able to give rise to all the pancreatic cell types, including beta cells, following implantation in mice [10]. Altogether, these findings suggest that mammalian pancreatic ducts possess the intrinsic capacity to (re)generate beta cells even though this process is poorly efficient and slow, especially in adults. In contrast to mammals, zebrafish possess remarkable capacity of regeneration, independently of its age [11]–[16]. This model can therefore be exploited to identify and characterize regenerative mechanisms and ultimately induce regeneration in mammals. Based on regenerative mechanisms identified in zebrafish, several studies succeed to improve regeneration in mammals, underlying the possibility of translation from zebrafish to mammals ([17]–[21] and [22], for review).

In zebrafish, the nitroreductase (NTR)/nitroaromatic prodrug system is widely used. In this technique, the combination of cell type-specific NTR expression and nitroaromatic prodrug exposure allow for controlled and targeted cell ablation [23], [24]. When NTR is expressed under the control of the *insulin* (*ins*) promoter (*Tg*(*ins:NTR-mCherry*) [25]), beta cell destruction is complete within 3 days following the treatment in adult fish, which correlate with a peak of hyperglycemia [26], [27]. The regeneration of beta cells upon ablation is spontaneous and fast and the glycemia is normalized within two weeks [13], [29]. Similar to mice, new beta cells can arise through proliferation of surviving beta cells [28] as well as through the contribution of alpha cells [29], [30] and delta cells[31], [32], underscoring the overall conservation of these processes from zebrafish to mammals. Nevertheless, unlike mammals, the presence of pancreatic progenitors in the ducts is well established in both larval [33] and adult zebrafish [26], [27]. Lineage tracing experiments pointed out that ductal cells and centroacinar cells (CACs) give rise to new beta cells [26], [33]. In adults, duct-derived beta cells start to be detected between 7 and 10 days following beta cell ablation [26], [27].

Notch signaling is a key player regulating the differentiation of duct-associated progenitors into endocrine cells. Larval duct cells as well as adult CACs display strong Notch activity [26], [34]. This signaling pathway has a central role in beta cell genesis during both development [35] and regeneration [33] by repressing endocrine differentiation. In zebrafish, different levels of Notch activity determine the behavior of the pancreatic progenitors. While a high level of Notch activity maintains cells in quiescence, a moderate level induces the entry in the cell cycle and proliferation whereas a low level drives endocrine differentiation of the progenitor cells [35]. A steep decrease of Notch activity pushes the progenitors to differentiate prematurely, bypassing the amplification step and leading to their depletion [35]. Repression of the Notch signaling by mTor, activated by glucose and nutrients, hence promotes beta cell formation and regeneration from ductal progenitors [33]. While Notch and mTor signaling are crucial for this process, there is still a need to establish a global view of the molecular mechanisms regulating beta cell regeneration.

93 To identify early events regulating ductal-derived beta cell regeneration, we determined the
94 transcriptomic signature of ductal cells from adult zebrafish following beta cell destruction. Our data
95 highlighted an upregulation of the Calcineurin (CaN) pathway. To elucidate CaN function in beta cell
96 regeneration, we both repressed and activated CaN pathway. We showed that CaN regulates beta cell
97 neogenesis in the ducts during regeneration, by modulating progenitor proliferation. Together, our
98 findings underline that CaN fine tunes the balance between progenitor proliferation and beta cell
99 differentiation to guarantee proper regeneration.

100

101 **Results**

102 *Transcriptomic profiling of ductal cells after beta cell destruction highlights regulation of calcineurin*
103 *pathway*

104 To gain a better understanding of the molecular mechanisms underlying the regeneration of beta cells
105 from the ducts, we determined the transcriptional landscape of ductal cells by RNA-sequencing after
106 beta cell ablation in adults. To selectively ablate the beta cells, we used the *Tg*(*ins:NTR-mCherry*)
107 transgenic fish and the ductal cells were labelled through the *Tg*(*nkx6.1:GFP*) reporter line [27] in which
108 GFP marks the ductal tree and associated multipotent pancreatic progenitors [27]. More precisely, 3
109 to 4 fishes were treated with the pro-drug MTZ at 10mM overnight, to induce ablation of beta cells or
110 with DMSO for the non-ablated controls. Ablation was confirmed by blood glucose measurement
111 before collection of the pancreas. To capture the early events triggered by the destruction of beta cells,
112 we generated the transcriptome of the ducts 3 days post ablation treatment (dpt), *i.e.* before beta cell
113 neogenesis. Differential gene expression analysis revealed that 1866 genes are up-regulated and 1515
114 genes down-regulated in the ductal cell of fish treated with MTZ compared to control (pAdj < 0.05).
115 According to Gene Ontology analysis, the most enriched pathways among the up-regulated genes were
116 DNA replication and cell cycle (**Figure 1A**). This further corroborates our previous findings and those of
117 others regarding the activation of duct-associated progenitors' proliferation in response to beta cell
118 ablation[26], [27]. As expected, the Notch pathway was enriched in the down-regulated genes [33],
119 [35] (**Figure 1B**). Intriguing in a context of strong proliferative response, we found an enrichment of
120 the cellular senescence signature (**Figure 1A**). We looked further in the genes associated with this
121 signature. Among them were found several components of the calcineurin signaling pathway such as
122 *nfatc3b*, *ppp3ccb* (the catalytic subunit of Calcineurin*), itpr2* and *calm3b* **(Figure 1C)**. In addition to
123 these genes related to cellular senescence, our RNAseq studies revealed the modulation of other genes
124 from the CaN canonical pathway (**Figure 1D, genes in green**), underlying its potential role in beta cell
125 regeneration. Calcineurin (CaN) is a highly conserved calcium/calmodulin dependent Ser/Thr

126 phosphatase, involved in numerous biological process including fin regeneration and beta cell function,
127 [36]–[39]. This prompted us to investigate the role of CaN in beta cell regeneration

128 Previous RNAseq data performed in our laboratory indicate that CaN (*ppp3cca/b*) and NFATc3
129 (*nfatc3a/b*) are mainly express in endocrine cells [40] (**Figure 1A supplemental**), which is in accordance
130 with the role of CaN/NFAT signaling in beta cells [41]. CaN genes (*ppp3cca/b*) as well as *nfatc3b,* are
131 express at lower levels in the ducts at basal state but their expression is induced in response to beta
132 cell destruction (**Figure 1B supplemental**).

133 *Calcineurin activity regulates the ductal regenerative response*

134 To evaluate the role of CaN in beta cell regeneration, more specifically derived from ductal progenitors,
135 we have chosen to use young larvae, where regenerated beta cells in the pancreatic tail arise
136 exclusively from the ducts [33]. In response to beta cells ablation, the intrapancreatic ducts undergo a
137 ductal regenerative response whereby differentiation toward the endocrine fate is increased [33]. We
138 first determined the rate of beta cell neogenesis from the ducts in response to a single acute ablation
139 of beta cells as we performed in adults. We treated *Tg*(*ins:NTR-P2A-mCherry*); *Tg*(*nkx6.1:GFP*) larvae
140 with nifurpirinol (NFP) from 3 to 4 dpf mCherry+ beta cells were quantified in the GFP+ ducts present
141 in the tail at several time points: 4, 7, 10 and 14 dpt (**Figure 1E**). Duct-associated beta cells started to
142 be detected in non-ablated larvae between 7 and 10 dpt (**Figure 1F**) and the number of beta cells slowly
143 increased until 14 dpt (**Figure 1F, 1G**). In ablated larvae, the increase became more pronounced from
144 10 dpt onwards (**Figure 1F, 1G**), indicating faster endocrine differentiation. This experiment establishes
145 that the ductal regenerative response is detectable between 10 and 14 days after the ablation of beta
146 cells, performed at 3 dpf. We next wanted to determine if ductal cell proliferation is activated in
147 response to beta cell destruction in larvae as in adult fish. We exposed *Tg(ins:NTR-P2A-mCherry);*
148 *Tg(nkx6.1:GFP)* larvae to EdU the second day following ablation (**Figure 1H**). In ablated larvae, the
149 proportion of GFP+ ductal cells EdU+ (in S-phase) was higher compared to non-ablated larvae (**Figure**
150 **1I, 1J**). This result shows that acute beta cell ablation in larvae rapidly activates ductal cell proliferation,
151 as previously reported in adult zebrafish.

152 As our transcriptomic data from adult zebrafish revealed modulation of CaN pathway at 3 dpt, we
153 treated *Tg*(*ins:NTR-P2A-mCherry*); *Tg*(*nkx6.1:GFP*) larvae from 1 to 3 dpt after beta cell ablation, with
154 a CaN inhibitor, the Cyclosporin A (CsA) [39] (**Figure 2A**). The number of newly formed beta cells was
155 monitored in the tail from 4 to 14 dpt. CsA enhanced beta cell formation at 10 dpt (**Figure 2B-D)**.
156 However, this effect appears to be transient since no discernible difference was observed between the
157 control and CsA-treated larvae in regeneration at the latest time point, suggesting an acceleration of
158 the regenerative response (**Figure 2B, Figure 2A supplemental**). Interestingly, CsA did not affect beta

159 cell differentiation in non-ablated larvae indicating that CsA only acts in a regenerative context (**Figure**
160 **2B-D)**. Of note, CsA increased as well the number of regenerated beta cells in the principal islet (**Figure**
161 **2B supplemental**).

162 We next tested the effect of CsA on endocrine progenitors in a regenerative context. We induced
163 regeneration in Tg(*neurod1:GFP*) larvae where the GFP is expressed in both endocrine progenitors and
164 mature endocrine cells. We first assessed generation of GFP cells at different time points (**Figure 2D**
165 **supplemental)** and showed that CsA induced an increase of neurod1+ cells from 4 dpt. The increase
166 was still detectable at least until 10dpt (**Figure 2E, Figure 2E supplemental**). To determine if these
167 additional cells result from their own proliferation, we performed a pulse of EdU just before analysis
168 (**Figure 2D supplemental**). We observed that CsA did not affect the neurod1+ proliferation rate that is
169 very low at these stages (**Figure 2F**). As a consequence, the effect of CsA cannot be explained by
170 endocrine cell proliferation but rather by neogenesis from progenitors. As CsA affects pro-endocrine
171 cells formation, we next wondered if the increased cell formation induced by CsA is specific to beta
172 cells. Treatment with CsA was performed as previously and delta and alpha cells were detected by
173 immunofluorescence. Interestingly, CsA did not affect alpha nor delta1.1 cells neogenesis in response
174 to beta cell ablation (**Figure 2F-G supplemental**). Overall, these experiments showed that CsA affects
175 specifically the beta cells and their endocrine progenitors.

176 *CaN over-activation abolishes the regenerative response*

177 We then wondered if an opposite regulation of CaN *i.e.* its activation impacts as well the regenerative
178 response. To that end, we generated a transgenic line Tg(*hsp70:GFP-P2A-ppp3ccCA*) that allows
179 ubiquitous expression of a constitutively active form of CaN^{CA} (*ppp3cc*^{CA}) upon heat shocks. Beta cell
180 ablation was triggered in Tg(*hsp70:GFP-P2A-ppp3cc*^{CA}); Tg(*ins:NTR-P2A-mCherry*); Tg(*nkx6.1:GFP*)
181 larvae from 3 to 4 dpf and CaN^{CA} expression was induced by four successive heat-shocks from 1 to 3
182 dpt (**Figure 3A**). The overexpression of CaN^{CA} after ablation impaired the regenerative response at 14
183 dpt (**Figure 3B-C**). Similar results were obtained with Tg(*UAS:GFP-P2A-ppp3cc*^{CA}); Tg(*cftr:gal4*)[45] ;
184 Tg(*ins:NTR-P2A-mCherry*) larvae in which CaN^{CA} is constitutively and specifically overexpressed in the
185 ducts within the pancreas (**Figure 3D-E**). Importantly, the structure of the ducts was similar in CaN^{CA}
186 overexpressing larvae compared to Tg(*nkx6.1:GFP*) controls (**Figure 3D**), suggesting that the
187 suppression of the regenerative response in CaN^{CA}-overexpressing larvae was not due to
188 morphogenetic defects during ductal growth. This result strongly suggest that CaN acts directly in the
189 ducts to regulate beta cell regeneration while it is not necessary for normal beta cell differentiation.

190 *CaN regulates beta cell differentiation induced by Notch inhibition in absence of regeneration*

191

192 Our transcriptomic data showed that the Notch pathway is downregulated in ductal cells during beta
193 cell regeneration (**Figure 1**). As the level of Notch activity determines the behavior of ductal cells [33]
194 from quiescence to proliferation and subsequently to beta cell differentiation, we tested whether
195 calcineurin acts together with the Notch pathway on a common pool of ductal progenitors. To inhibit
196 the Notch pathway, we treated larvae with several concentrations of the gamma-secretase inhibitor
197 LY411575 from 3 to 4dpf in absence of regeneration. The activity of CaN was inhibited by CsA during
198 the same timeframe (**Figure 4A**). As previously, we used reporter lines for beta and ductal cells
199 *Tg*(*ins:NTR-P2A-mCherry*); *Tg*(*nkx6.1:GFP*) and the number of secondary beta cells was analyzed at
200 6dpf (**Figure 4A**). As expected, the number of beta cells progressively rose as the concentration of the
201 Notch inhibitor increased (**Figure 4B**). Combined treatment with CsA fostered the differentiation of
202 beta cells between 1 and 10 µM LY411575 but did not result in further increase at 15 µM LY411575
203 (**Figure 4B**), suggesting that CaN is important within a permissive window of Notch activity. Since we
204 overserved the highest synergistic effect at 5µM of LY411575, we used this concentration for the
205 following experiments (**Figure 4C-D**). It is worth noting that combined treatment of LY411575 (5uM)
206 and another CaN inhibitor, FK506, resulted in the same synergistic increase of beta cell differentiation
207 (**Figure 4A-B supplemental**), confirming that the effect is due to CaN inhibition. The combined effect
208 of Notch and CaN inhibition is transient as it is not observed at 7dpf anymore (**Figure 4E**). Therefore,
209 as observed in regenerative conditions (**Figure 2B**), CaN inhibition accelerates beta cell neogenesis
210 induced by Notch repression.

211 To determine to which extent CaN pathway can modulate Notch induced beta cell neogenesis, we
212 activated CaN^{CA} overexpression in *Tg*(*hsp70:GFP-P2A-ppp3cc*^{CA}*); Tg*(*ins:NTR-P2A-mCherry*) larvae by an
213 heat-shock at 3 dpf and treated them with LY411575 (**Figure 4C supplemental)**. CaN^{CA} overexpression
214 resulted in a lowered beta cell formation induced by Notch inhibition (**Figure 4D supplemental**),
215 revealing that CaN activation counterbalanced the effects of Notch inhibition. Using our previous
216 settings of Notch and CaN inhibition, we next wondered if the canonical pathway downstream of CaN
217 was involved in the enhancement of beta cell differentiation. To activate NFAT, a well-known target
218 of CaN, we used CHIR99021 allowing a stabilization of the active form of NFAT (**Figure 1D**). We found
219 that CHIR99021 rescued the effect of CsA (**Figure 4D supplemental**), suggesting that CaN inhibition
220 increases beta cell neogenesis at least partially by the regulation of NFAT. Overall, these results reveal
221 that CaN regulates beta cell formation in pro-endocrinogenic context, such as induced by a low level
222 of Notch activity. Moreover, it suggests that both CaN and Notch pathway act on a common pool of
223 ductal progenitors to regulate beta cell neogenesis.

224

225 *CaN controls the proliferation of duct-associated progenitors induced by Notch inhibition*

226

227 Given that we observed the most significant increase in beta cell formation with CsA when Notch
228 activity was mildly repressed (**Figure 4B-D**), and since mild Notch activity has been shown to promote
229 progenitor amplification [35], it suggests that CaN acts at this level. To explore this possibility, we
230 exposed briefly *Tg*(*nkx6.1:GFP*) larvae to EdU after mild Notch (LY411575 5µM) and CaN inhibition
231 (**Figure 5A**). As expected, Notch inhibition increased the proportion of proliferating EdU+ GFP+ duct
232 cells at 4dpf (**Figure 5B-C**) and decreased the amount of ductal progenitors 2 days later (**Figure 5D**),
233 which is concomitant with the increase of beta cell differentiation (**Figure 4C-D**). Interestingly, the
234 combined inhibition with CsA further increased these proportions (**Figure 5B-D**). In contrast, CaN
235 inhibition alone had no effect on basal proliferation or on the number of ductal progenitors (**Figure**
236 **5B-D**). Incidentally, at 4dpf, while the proliferation is increased (**Figure 5C**), the number of ductal cells
237 remained the same in all conditions (**Figure 5A supplemental**), suggesting that ductal cells have not
238 yet left the cell cycle to differentiate. In comparison, after stronger Notch inhibition (15µM), the ductal
239 cells are already depleted at 4dpf (**Figure 5B supplemental**), as they directly differentiate without
240 entering the cell cycle [35]. In these conditions, CsA could therefore not enhance ductal progenitor
241 proliferation and thus beta cell formation (**Figure 4B**). These results show that CaN and Notch
242 pathways act together on the proliferation of the ductal progenitors to prevent their exhaustion.

243 *CaN prevents exhaustion of Notch responsive progenitors during beta cell regeneration*

244

245 Taken together, our results indicate that CaN plays a role in regulating the proliferation of ductal
246 progenitors in contexts that are permissive for beta cell differentiation. To demonstrate that CaN
247 regulates ductal progenitor proliferation in a similar manner to Notch inhibition but during
248 regeneration, we exposed *Tg(ins:NTR-P2A-mCherry*); *Tg(nkx6.1:GFP*) larvae after ablation and CsA
249 treatment (**Figure 5E**). CaN inhibition enhanced the proliferation of ductal cells in ablated larvae
250 (**Figure 5F-G**). To next determine if CaN acts on the Notch-responsive progenitors in beta cell
251 regeneration, we then used *Tg(tp1:VenusPest)* Notch reporter line. At larval stages the vast majority
252 of ductal cells are Notch responsive and the reporter line marks all the progenitors within the ductal
253 tree [34]. We treated *Tg(ins:NTR-P2A-mCherry*); *Tg(tp1:VenusPest)* as described above (**Figure 5E**). In
254 ablated-larvae, CsA increased tp1+ ductal cell proliferation (**Figure 5H-I**). Moreover, CsA induced a
255 reduction of tp1+ ductal cells in ablated larvae (**Figure 5 H-J**), suggesting an exhaustion of the Notch
256 responsive progenitors, in accordance with premature beta cell differentiation we observed (**Figure**
257 **2B-4D**). Lastly, CsA does not affect tp1+ cells in non-ablated larvae showing that CaN inhibition did not

258 directly affect Notch signaling (**Figure 5J**). Those results suggest that CaN fine tunes the balance
259 between proliferation of the progenitors and their differentiation to prevent their exhaustion during
260 beta cell regeneration.

261 *CaN regulation is functionally relevant in adult zebrafish*

262 To further expand upon our findings and investigate their relevance in a non-developmental context,
263 we next ought to determine whether CaN function is maintained in older zebrafish. We used 2 months
264 old *Tg*(*ins:NTR-P2A-mCherry*); *Tg*(*nkx6.1:GFP*) juveniles fish to perform beta cell ablation followed by
265 CsA treatments. We analyzed the number of small islets (up to 5 cells) at 7 and 10dpt. At 7dpt, CsA
266 increased the number of small islets in ablated larvae (**Figure 6A-B**) showing that CaN inhibition
267 enhances beta cell regeneration in juvenile zebrafish, as in larvae. It is noteworthy that, as in larvae,
268 we highlighted an acceleration of beta cell regeneration. The increase number of small islets is indeed
269 transient as it not observe anymore at 10dpt (**Figure 6C**).

270 Next, we determined the functional impact of CaN overexpression or inhibition by assessing the
271 glycemia at 7, 10 and 14 after beta cell ablation. Overexpression of CaN^{CA} using either *Tg(hsp70:GFP-*
272 *P2A-ppp3cc*^{CA}*)* or *Tg*(*cftr:gal4*); *Tg*(*UAS:GFP-P2A-ppp3cc*^{CA}*), led to an increased glycemia at both 7 and*
273 *10dpt* (**Figure 6D-E)***,*** before recovery at 14 dpt (**Figure 6A supplemental**). This indicates that the
274 overexpression of CaN impedes the recovery of glycemia induced by beta cell regeneration. However,
275 CaN inhibition did not seem to further improve the glycemia (**Figure 6D-E**) probably because the
276 glycemia was already low at 7dpt (77 mg/dL on average) compared to non-ablated control (mg/dl)
277 (**Figure 6D-E**). Altogether, these results show that in adult zebrafish also, CaN regulation is necessary
278 to enable beta cell regeneration and for proper recovery of the glycemia after beta cell loss.

279 **Discussion**

280 The present study reveals the importance of the protein phosphatase CaN as a new player in beta cell
281 regeneration in zebrafish. We demonstrate that CaN act on ductal-associated progenitor cells by
282 balancing proliferation and endocrine differentiation. In addition, we show the interplay between CaN
283 and Notch signalling, a master regulator of beta cell regeneration.

284 Previous drug and genetic screening using zebrafish larvae enabled the identification of several
285 regulators of beta cell regeneration from different pancreatic cellular sources. For example, adenosine
286 has been shown to stimulate beta cell replication [28] and , igfbp1a [42] and TGFb suppression [30]
287 promote alpha-to-beta cell transdifferentiation. As for cdk5 inhibition and folinic acid/Folr1, they
288 promote beta cell regeneration from the pancreatic ducts [43], [44]. Here, to identify novel regulators
289 of beta cell regeneration specifically from pancreatic ducts, we carried out a transcriptomic profiling

290 of duct cells following beta cell ablation in the adult zebrafish. Transcriptomic analyses show that the
291 regulated genes encompass most of the genes and pathways identified in previous studies (igfbp1,
292 mTor, Notch, etc.), underlying the importance of those actors in beta cell regeneration. Our data reveal
293 also that DNA replication is the most enriched signature attesting that duct cells undergo a potent
294 proliferative response after the destruction of beta cells.

295 Besides these expected signatures, our transcriptomic data uncover the unanticipated upregulation of
296 numerous genes implicated in DNA repair and cell cycle arrest. These signatures might indicate that
297 highly proliferating ductal cells activate counteracting mechanisms. Among the genes regulated in
298 those signatures, we focused on CaN and determined its role in beta cell regeneration.
299 Pharmacological inhibition of CaN increases the proliferation of duct cells induced by beta cell ablation,
300 resulting in an acceleration of beta cell regeneration in the ducts. Consistently, transgene-mediated
301 CaN overactivation abolishes the regenerative response. Importantly, the inhibition of regeneration is
302 observed when CaN is overexpressed either ubiquitously or selectively in *cftr*-expressing ductal cells
303 indicating that the role of CaN in beta cell regeneration is intrinsic to the ducts. Based on functional
304 assays in larvae, we not only confirm the activation of the proliferation of ductal cells soon after beta
305 cell ablation, but also that the rate of progenitor proliferation is carefully controlled by CaN in order to
306 achieve proper and timely regeneration of beta cells. Our data are consistent with earlier studies
307 reporting a role of CaN in proliferation dynamics during fin regeneration. In the regenerating fin, low
308 CaN activity is found in the proximal region of the blastema characterized by a high rate of proliferation
309 and regeneration and its activity increases distally where lower proliferation is observed [36], [38],
310 [39]. It was suggested that CaN control blastemal cell progeny divisions [36]. In human, the importance
311 of CaN in proliferation is also highlighted in organ transplanted patients. When patients are treated
312 with Cyclosporin A (*i.e.* the CaN inhibitor we used in this study) as immunosuppressive drug they
313 indeed present an increased risk of skin cancer, notably due to keratinocyte senescence inhibition [45].

314 It has been shown that Notch inhibitory treatments switch progenitors from proliferative self-renewing
315 to premature differentiation, leading to progenitor depletion [34], [35]. Our study reveals that this
316 phenomenon is further exacerbated by CaN inhibition. Importantly, during normal larval development
317 in absence of Notch inhibitory treatment, CaN does not affect basal ductal proliferation nor beta cell
318 differentiation. Hence, Notch signalling has to be repressed to detect the effect of CaN on the
319 progenitors, suggesting that CaN acts downstream of Notch pathway. In differentiating keratinocytes,
320 CaN cooperates with Notch signalling to regulate p21/*cdkn1a* (which is upregulated in the ducts at 3
321 dpt), cell cycle withdrawal and differentiation [46]. These studies show that CaN acts in association
322 with Notch signalling on progenitors proliferation and on their differentiation.

323 Based on our data, we build the model depicted in Figure 7A. Our study suggests that CaN acts in
324 competent progenitor cells and that this competence is determined by Notch signalling. When Notch
325 is repressed to a mild level, the progenitor enter into the cell cycle and acquire a pro-endocrinogenic
326 competence [35]. CaN acts on these progenitors to tone down an excessive proliferation and avoid the
327 exhaustion of these progenitors. CaN is therefore a guardian of the progenitor population. CaN
328 inhibition both increases progenitor proliferation and induces their depletion, suggesting a switch to a
329 symmetric division resulting in two daughter cells entering in endocrine differentiation.

330 More precisely, a previous study in mice uncover the existence of three division modes of the
331 pancreatic progenitors during embryonic development, *i.e.* symmetric self-renewing resulting in two
332 progenitors cells ; asymmetric resulting in a progenitor and a endocrine cell and symmetric
333 differentiative resulting in two differentiated cells [47]. The authors actually show that the type of
334 division is defined by the timing of induction of endocrine program by NEUROG3 [47]. Interestingly,
335 NEUROG3 seems to be the link between proliferation and differentiation, and its expression is
336 regulated by Notch signalling [48]. In zebrafish, endocrine differentiation is not induced by *Neurog3*
337 but by *Ascl1b* and *Neurod1* [49]. Concerning that subject, CaN inhibition accelerates the formation of
338 neurod1+ cells. Hence CaN could possibly act via the determination of the type of division *i.e.*
339 symmetric vs asymmetric. This model is supported by previous observation in others systems. In stem
340 cells and neuronal and hematopoietic progenitors, premature differentiation results from a switch in
341 the mode of cellular division, from symmetric amplifying division to asymmetric differentiating division
342 [50], [51]. Notch determines the choice between both types of divisions [52], [53].

343 Calcineurin is known to be implicated in cellular senescence [45]. Usually thought as negative
344 regulators of development and cellular growth, DNA repair [54] and cellular senescence [55] appear
345 to be required in both developmental and regenerative processes. Our transcriptomic data suggest
346 that these mechanisms are required for beta cell regeneration. Therefore, it would be interesting to
347 determine the contribution of these cellular processes in the ductal progenitors and determine if CaN
348 acts via cellular senescence in this case.

349 Overall, this study brings new insights on beta cell regeneration and highlights the ductal progenitor
350 cell cycle as a cornerstone in the process. Some studies report an increase of proliferation of some
351 ductal cell population in diabetic patients [10], [56], implying a regenerative response. However, these
352 ductal cells cannot efficiently reform the beta cell mass, suggesting a dormant mechanism of
353 regeneration. As such, the balance between proliferation and induction of endocrine differentiation
354 could be a key to improve beta cell neogenesis. However, as CaN is also important for beta cell
355 function, this approach would require to be transient to induce neogenesis. Therefore, it should be

combined with methods to induce beta cell proliferation to ultimately reconstitute the beta cell mass. Overall, this study brings a better understanding on the regulation of the balance between ductal progenitors proliferation and endocrine differentiation. These results should provide new hints to help improve regenerative competences in mammals.

Material and Methods

Key resources table

Reagent type or resource	Designation	Source or reference	Identifier	Additional information
Genetic reagent (Danio rerio)	*TgBAC(nkx6.1:eGFP)^{ulg004}*	PMID: 26329351	ZFIN: ZDB-ALT-160205-1	
Genetic reagent (Danio rerio)	*Tg(ins:NTR-P2A-mCherry)^{ulg034}*	PMID: 29663654	ZFIN: ZDB-ALT-171122-9	
Genetic reagent (Danio rerio)	*Tg(cftr:gal4)*	PMID: 25592226	ZFIN : ZDB-FISH-150901-25442	
Genetic reagent (Danio rerio)	*Tg(tp1:VenusPest)*	PMID: 22492351	ZFIN: ZDB-FISH-150901-8023	
Genetic reagent (Danio rerio)	*Tg(hsp70:eGFP-P2A-ppp3ccaCA) ^{ulg068}*	This paper		See Zebrafish husbandry and generation of the *Tg(hsp70:eGFP-P2A-ppp3ccaCA) zebrafish line*
Genetic reagent (Danio rerio)	*Tg(UAS:eGFP-P2A-ppp3ccaCA) ^{ulg069}*	This paper		See Zebrafish husbandry and generation of the *Tg(UAS:eGFP-P2A-ppp3ccaCA) zebrafish line*
Antibody	Anti-GFP (chicken polyclonal)	Aves Labs	GFP-1020	1:1000
Antibody	anti-mCherry/dsRed (Living Colors Polyclonal)	Clontech	632496	1:500
Antibody	Anti-glucagon (mouse polyclonal)	Sigma	G2654	1:300
Antibody	Goat anti-Chicken IgY (H+L), Alexa Fluor™ 488	Invitrogen	A-11039	1:750
Antibody	Goat anti-dsred 568	Invitrogen		1:750

Antibody	Goat anti-Mouse IgG (H+L) Cross-Adsorbed Secondary Antibody, Alexa Fluor 633	Invitrogen		1:750
Chemical compound	Nifurpirinol (NFP)	Sigma-Aldrich	32439	
Chemical compound	Metronidazole (MTZ)	Sigma-Aldrich	M1547	
Chemical compound	Cyclosporine A (CsA)	Selleckchem	S2286	
Chemical compound	LY411575	Sigma-Aldrich	SML0506	
Chemical compound	CHIR990211	Sellekchem	CT99021	
Commercial assay or kit	Gateway™ LR Clonase™ II Enzyme mix	Invitrogen	11791020	
Commercial assay or kit	Gateway™ BP Clonase™ II Enzyme mix	Invitrogen	11789020	
Sequence based reagent	IM369	This paper	PCR primer	gaagaaaaccccggtcctatgtcgacgaaagagccgaaag
Sequence based reagent	IM380	This paper	PCR primer	ccttacacattcccgtcagtgc
Sequence based reagent	IM371	This paper	PCR primer	CGGCTCTTTCGTCGACATAGGACCGGGGTTTTCTTCCACG
Sequence based reagent	O226	This paper	PCR primer	GCCACCATGGTGAGCAAGGGCGAGGA
Sequence based reagent	IM370	This paper	PCR primer	ttattagatcttatttctgatcacctcctt
Sequence based reagent	IM459	This paper	PCR primer	cacacgaattcgccgccaccATGGTGAGCAAGGGCGAG
Sequence based reagent	IM460	This paper	PCR primer	ggatcggtcgagatccttacGATCTTATTTCTGATCACCTCCTTACG
Sequence based reagent	IM457	This paper	PCR primer	GTAAGGATCTCGACCGATCCTG
Sequence based reagent	IM458	This paper	PCR primer	GGTGGCGGCGAATTCGTG
Commercial assay or kit	Nextera® XT DNA Library kit	Illumina	FC-131-1024	
Commercial assay or kit	Click-iT™ EdU Cell Proliferation Kit for Imaging, Alexa Fluor™ 647 dye	Invitrogen	C10340	

Software, algorithm	Imaris	Bitplane (http://www.bitplane.com/imaris/imaris)	RRID:SCR_007370	Version 9.5
Software, algorithm	GraphPad Prism	GraphPad Prism (https://graphpad.com)	RRID:SCR_015807	Version 8
Software, algorithm	DESeq2	DESeq2 (https://bioconductor.org/packages/release/bioc/html/DESeq2.html)	RRID:SCR_015687	
Software, algorithm	WebGestalt	WebGestalt (http://www.webgestalt.org/)	RRID:SCR_006786	

Zebrafish husbandry and generation of the Tg(hsp70:eGFP-P2A-ppp3ccaCA)^{ulg068} and Tg(UAS:eGFP-P2A-ppp2ccaCA)^{ulg069} zebrafish lines

Tg BAC(nkx6.1:eGFP)^{ulg004} [57] *; Tg(ins:NTR-P2A-mCherry)^{ulg034}* [58] *; Tg(cftr:gal4)* and *Tg(tp1:VenusPest)* were used. Zebrafish were raised in standard conditions at 28°C. All experiments were carried out in compliance with the European Union and Belgian law and with the approval of the ULiège Ethical Committee for experiments with laboratory animals (approval number : 2075).

The *hsp70:GFP-P2A-ppp3ccaCA* transgene has been generated by cloning a PCR fragment containing the Gateway vector pCR8/GW/TOPO. Firstly, we amplified the full length of ppp3ccaCA with primers IM369/IM380 and amplified *GFP-P2A* with overlapping regions with IM371/O226. The overlapping PCR used the primers O226/IM380. Then to obtain a truncated *ppp3ccaCA* lacking the calmodulin biding and the autoinhibitory domain, resulting in a constantly active form of calcineurin, we amplified the last fragments with IM370/O226 and cloned into PCR8 vector. The promoter was assembled by LR recombination with pE5-hsp70 into pDestTol2p2A from the Tol2kit [59]. *Tg (hsp70:GFP-P2A-ppp3ccaCA)* fish have been generated using the Tol2 mediated transgenesis [60]. *The Tg(UAS:GFP-P2A-ppp3ccacA*) has been generated by ligation (KLD kit, NEB) of PCR fragments *GFP-P2A-ppp3ccacA (*IM459/IM460) with the UAS sequences (IM457/IM458) in plasmid from (Distel 2009) and then

381 inserted into pDestTol2p2A from the Tol2kit. Final constructions has been injected with transposase
382 into wild type (WT) AB embryos.
383
384 *Beta-cell ablation*

385 Adults fish for RNA-sequencing experiment were treated with freshly prepared metronidazole (MTZ)
386 (Sigma M1547) at 10mM with 0.2% DMSO in fish water. Control treatments consisted of fish water
387 containing 0.2% DMSO. Fish were treated for 18 hours in the dark. Nifurpirinol (NFP) (32439, Sigma-
388 Aldrich) stock solution was dissolved at 2.5 mM in DMSO. b-cell ablation in *Tg(nkx6.1:eGFP);*
389 *Tg(ins:NTR-P2A-mCherry)* larvae was induced by treatment with 2.5 µM NFP in E3. Control treatments
390 consisted of E3 containing 0.2% DMSO. Larvae were treated for 18 hours in the dark.

391 *Drug treatments*

392 Cyclosporine A (Selleckchem, S2286), CHIR99021 and LY411575 (Sigma-Aldrich, SML0506) stock
393 solution were dissolved at 10mM in DMSO. Larvae treatment were respectively performed at 0.1 µM
394 and 5µM in E3. Control treatments consisted of E3 containing the same amount of DMSO than drug
395 treatment. Larvae were treated for 18 hours in the dark.

396 *5-ethynyl-2'-deoxyuridine (EdU) incorporation assay*

397 Zebrafish larvae were incubated in 4 mM EdU dissolved in E3 water for 8 hours, they were then directly
398 euthanised in tricaine and fixed in 4% PFA. EdU was detected according to the protocol of Click-iT™
399 EdU Cell Proliferation Kit for Imaging, Alexa Fluor™ 647 (ThermoFisher C10340) after whole mount
400 immunodetection.

401 *Heat Shock*

402 *Successive heat shocks of 30 minutes and 12 hours apart were performed at 39°C for larvae and 37°C*
403 *for juveniles and adults zebrafish.*

404 *Whole mount immunodetection*

405 Larvae were euthanized in tricaine and fixed in 4% PFA at 4 °C for IHC. The digestive tract of juveniles
406 was dissected prior immunodetection and kept in methanol for at least 18 hours. After depigmentation
407 with 3% H2O2/1% KOH, larvae were permeabilised 30 min in PBS/ Triton X-100 and incubated for two
408 hours in blocking buffer (4% goat serum/1% BSA/PBS/0.1% Triton X-100). Primary and secondary
409 antibodies were incubated at 4 °C overnight.

	Fixation duration	Depigmentation duration	Permeabilization solution	Permeabilization duration
5-10 dpf	18 hours	15 min	PBTr 0.05%	30 min
13-17 dpf	36 hours	20 min	PBTr 2%	30 min
2months (digestive tract)	18 hours	15 min	/	/

410

411 Primary antibodies: Living Colors Polyclonal anti-mCherry/dsRed (rabbit, 1:500, Clontech 632496),
412 anti-GFP (chicken, 1:1000),

413 Secondary antibodies: Alexa Fluor-488, -568, -633 (goat, 1:750, Molecular Probes).

414 *Flow cytometry and FACS*

415 The whole pancreas from 3-4 fish of *Tg(nkx6.1:eGFP); Tg(ins:NTR-P2A-mCherry)* adult fish (6–10
416 months old, males and females) were dissected, collected and washed in HBSS without Ca^{2+}/Mg^{2+}. Live
417 cell dissociation was performed in Tryple Select 1x solution (GIBCO) supplemented with 100 U/mL
418 collagenase IV (Life Technologies 17104-019) and 40 µg/mL proteinase K (Invitrogen, 25530031) for 10
419 min at 28 °C.

420 The GFP+ cells were selected on FACS Aria III and sorted under purity mode and after exclusion of the
421 doublets. The purity of the sorted cells was confirmed by epifluorescence microscopy (~95 %). Cells
422 (about 1000-5000/fish depending on the cell type) were immediately lysed with 0.5% Triton X-100
423 containing 2U/µl RNAse inhibitor and stored at –80 °C.

424 *mRNA sequencing of FACSed cells and bioinformatic analyses*

425 cDNAs were prepared from lysed cells according to SMART-Seq2.0 (Picelli et al., 2014) for low input
426 RNA sequencing and libraries were prepared with Nextera® DNA Library kit (Illumina). Independent
427 biological replicates of each cell type sequenced using Illumina NextSeq500 and obtained ~20 million
428 100 bp paired-end reads. Reads were mapped and aligned to the zebrafish genome GRCz11 from
429 Ensembl gene annotation version using STAR version 2.6.1 (Dobin et al., 2013). Gene expression levels
430 were calculated with featureCounts (http://bioinf.wehi.edu.au/featureCounts/) and differential
431 expression determined with DESeq2 (Love, Huber, & Anders, 2014). Expression values are given as
432 normalized read counts. Poorly expressed genes with mean normalized expression counts <10 were
433 excluded from the subsequent analyses. DESeq2 uses Wald test for significance with posterior
434 adjustment of P values (Padj) using Benjamini and Hochberg multiple testing. The differentially
435 expressed (DE) genes identified with a Padj cutoff of 0.05 were submitted for GO analysis using
436 WebGestalt tool (Liao, Wang, Jaehnig, Shi, &Zhang, 2019).

437 *Confocal microscopy and image analysis*

438 Images were acquired using Leica SP5 confocal microscope. We used ImageJ to count the cells and
439 Imaris to do the pictures.

440 *Glycemia measurement*

441 *Glycemia measurement were performed as described in* [58].

442 **Data availability**

443 The sequences that support the findings are of this study have been deposit in Geo with the accessions
444 codes GSE212124, https://www.ncbi.nlm.nih.gov/geo/info/linking.html. The authors declare that all
445 other data supporting the findings of this study are available within the paper and its supplementary
446 information files.

447 **Authors contribution**

448 **L.M.** conducted experiments, acquired and analysed data, analysed transcriptomic data, wrote the
449 manuscript. **D.B.** conducted RNA-seq experiment and revised the manuscript **A.L.** implemented
450 bioinformatic programs and analysed transcriptomic data. **C.R., C.G. and C.D.** conducted experiments.
451 **L.F.** revised the manuscript. **B.P.** provided resources and advised on research studies. **M.L.V.** provided
452 resources, advised on research studies and revised the manuscript **I.M.** supervised the whole work,
453 acquired funding, designed the research studies, verified data and assisted in writing the manuscript.

454 **Acknowledgments**

455 The authors thank the GIGA technology platforms GIGA-Genomics and GIGA-Imaging. The authors also
456 thanks Jérémie Zappia for critically reading the manuscript, Jordane Bourdouxhe and Marie Alice
457 Dupont for their help with the constructions.

458 **Duality of interest**

459 No potential conflicts of interest.

460 **References**

461 [1] Y. Dor, J. Brown, O. I. Martinez, and D. a Melton, "Adult pancreatic beta-cells are formed by
462 self-duplication rather than stem-cell differentiation.," *Nature*, vol. 429, no. model 3, pp. 41–
463 46, 2004, doi: 10.1038/nature02520.

464 [2] F. Thorel *et al.*, "Conversion of Adult Pancreatic alpha-cells to Beta-cells after Extreme Beta
465 Cell Loss," *Nature*, vol. 464, no. 7292, pp. 1149–1154, 2010, doi:
466 10.1038/nature08894.Conversion.

467 [3] S. Chera *et al.*, "Diabetes recovery by age-dependant conversion of pancreatic delta-cells into
468 insulin producers," *Nature*, vol. 514, no. 7523, pp. 503–507, 2014, doi:
469 10.1038/nature13633.Diabetes.

470 [4] X. Xu *et al.*, "Beta Cells Can Be Generated from Endogenous Progenitors in Injured Adult
471 Mouse Pancreas," *Cell*, vol. 132, pp. 197–207, 2008, doi: 10.1016/j.cell.2007.12.015.

472 [5] M. Solar *et al.*, "Pancreatic Exocrine Duct Cells Give Rise to Insulin-Producing β Cells during
473 Embryogenesis but Not after Birth," *Dev. Cell*, vol. 17, pp. 849–860, 2009, doi:
474 10.1016/j.devcel.2009.11.003.

475 [6] H. Zhao *et al.*, "Pre-existing beta cells but not progenitors contribute to new beta cells in the
476 adult pancreas," *Nat. Metab.*, vol. 3, no. 3, pp. 352–365, 2021, doi: 10.1038/s42255-021-

477 00364-0.

478 [7] J. L. Kopp *et al.*, “Sox9+ ductal cells are multipotent progenitors throughout development but
479 do not produce new endocrine cells in the normal or injured adult pancreas,” *Development*,
480 vol. 138, pp. 653–665, 2011, doi: 138/4/653 [pii].

481 [8] M. Courtney *et al.*, “The Inactivation of Arx in Pancreatic α-Cells Triggers Their Neogenesis and
482 Conversion into Functional β-Like Cells,” *PLoS Genet.*, vol. 9, no. 10, pp. 1–18, 2013, doi:
483 10.1371/journal.pgen.1003934.

484 [9] C. Gribben *et al.*, “Ductal Ngn3-expressing progenitors contribute to adult β cell neogenesis in
485 the pancreas,” *Cell Stem Cell*, vol. 28, no. 11, pp. 2000-2008.e4, 2021, doi:
486 10.1016/j.stem.2021.08.003.

487 [10] M. M. F. Qadir *et al.*, “Single-cell resolution analysis of the human pancreatic ductal
488 progenitor cell niche,” *Proc. Natl. Acad. Sci. U. S. A.*, vol. 117, no. 20, pp. 10876–10887, 2020,
489 doi: 10.1073/pnas.1918314117.

490 [11] J. B. Moss, P. Koustubhan, M. Greenman, M. J. Parsons, I. Walter, and L. G. Moss,
491 “Regeneration of the pancreas in adult zebrafish,” *Diabetes*, vol. 58, no. August, pp. 1844–
492 1851, 2009, doi: 10.2337/db08-0628.

493 [12] K. D. Poss, L. G. Wilson, and M. T. Keating, “Heart regeneration in zebrafish,” *Science (80-.).*,
494 vol. 298, no. 5601, pp. 2188–2190, 2002, doi: 10.1126/science.1077857.

495 [13] T. Y. Choi, N. Ninov, D. Y. R. Stainier, and D. Shin, “Extensive conversion of hepatic biliary
496 epithelial cells to hepatocytes after near total loss of hepatocytes in zebrafish,”
497 *Gastroenterology*, vol. 146, no. 3, pp. 776–788, 2014, doi: 10.1053/j.gastro.2013.10.019.

498 [14] Y. Goldshmit, T. E. Sztal, P. R. Jusuf, T. E. Hall, M. Nguyen-Chi, and P. D. Currie, “Fgf-dependent
499 glial cell bridges facilitate spinal cord regeneration in zebrafish.,” *J. Neurosci.*, vol. 32, no. 22,
500 pp. 7477–7492, May 2012, doi: 10.1523/JNEUROSCI.0758-12.2012.

501 [15] V. Kroehne, D. Freudenreich, S. Hans, J. Kaslin, and M. Brand, “Regeneration of the adult
502 zebrafish brain from neurogenic radial glia-type progenitors,” *Development*, vol. 138, no. 22,
503 pp. 4831–4841, 2011, doi: 10.1242/dev.072587.

504 [16] M. Gemberling, T. J. Bailey, D. R. Hyde, and K. D. Poss, “The zebrafish as a model for complex
505 tissue regeneration,” *Trends Genet.*, vol. 29, no. 11, pp. 611–620, 2013, doi:
506 10.1016/j.tig.2013.07.003.

507 [17] C. Papadimitriou *et al.*, “3D Culture Method for Alzheimer’s Disease Modeling Reveals
508 Interleukin-4 Rescues Aβ42-Induced Loss of Human Neural Stem Cell Plasticity,” *Dev. Cell*, vol.
509 46, no. 1, pp. 85-101.e8, 2018, doi: 10.1016/j.devcel.2018.06.005.

510 [18] V. Mashkaryan *et al.*, “Type 1 Interleukin-4 Signaling Obliterates Mouse Astroglia in vivo but
511 Not in vitro,” *Front. Cell Dev. Biol.*, vol. 8, no. February, pp. 1–16, 2020, doi:
512 10.3389/fcell.2020.00114.

513 [19] S. Ko, T. Choi, J. O. Russell, J. So, and D. Shin, “Bromodomain and extraterminal (BET) proteins
514 regulate biliary-driven liver regeneration,” *J. Hepatol.*, vol. 64, no. 2, pp. 316–325, 2016, doi:
515 10.1016/j.jhep.2015.10.017.Bromodomain.

516 [20] Y. Goldshmit *et al.*, “Decreased anti-regenerative effects after spinal cord injury in spry4-/-
517 mice.,” *Neuroscience*, vol. 287, pp. 104–112, Feb. 2015, doi:
518 10.1016/j.neuroscience.2014.12.020.

519 [21] B. V. Fausett, J. D. Gumerson, and D. Goldman, “The proneural basic helix-loop-helix gene
520 Ascl1a is required for retina regeneration,” *J. Neurosci.*, vol. 28, no. 5, pp. 1109–1117, 2008,
521 doi: 10.1523/JNEUROSCI.4853-07.2008.

522 [22] L. Massoz, M. A. Dupont, and I. Manfroid, “Zebra-fishing for regenerative awakening in
523 mammals,” *Biomedicines*, vol. 9, no. 1, pp. 1–18, 2021, doi: 10.3390/biomedicines9010065.

524 [23] H. Pisharath, “Validation of nitroreductase, a prodrug-activating enzyme, mediated cell death
525 in embryonic zebrafish (Danio rerio),” *Comp. Med.*, vol. 57, no. 3, pp. 241–246, 2007.

526 [24] S. Curado, R. M. Anderson, B. Jungblut, J. Mumm, E. Schroeter, and D. Y. R. Stainier,
527 “Conditional targeted cell ablation in zebrafish: A new tool for regeneration studies,” *Dev.
528 Dyn.*, vol. 236, no. February, pp. 1025–1035, 2007, doi: 10.1002/dvdy.21100.

529 [25] H. Pisharath, J. M. Rhee, M. a Swanson, S. D. Leach, and M. J. Parsons, “Targeted ablation of
530 beta cells in the embryonic zebrafish pancreas using E.coli nitroreductase,” *Mech Dev.*, 2007,
531 doi: 10.1016/j.mod.2006.11.005.Targeted.

532 [26] F. Delaspre *et al.*, “Centroacinar cells are progenitors that contribute to endocrine pancreas
533 regeneration,” *Diabetes*, vol. 64, no. October, pp. 3499–3509, 2015, doi: 10.2337/db15-0153.

534 [27] A. P. Ghaye *et al.*, “Progenitor potential of nkx6.1-expressing cells throughout zebrafish life
535 and during beta cell regeneration,” *BMC Biol.*, vol. 13, p. 70, 2015, doi: 10.1186/s12915-015-
536 0179-4.

537 [28] O. Andersson *et al.*, “Adenosine signaling promotes regeneration of pancreatic β- cells in
538 vivo,” *Cell Metab.*, 2012, doi: 10.1016/j.cmet.2012.04.018.Adenosine.

539 [29] L. Ye, M. A. Robertson, D. Hesselson, D. Y. R. Stainier, and R. M. Anderson, “Glucagon is
540 essential for alpha cell transdifferentiation and beta cell neogenesis,” *Dev.*, vol. 142, no. 8, pp.
541 1407–1417, 2015, doi: 10.1242/dev.117911.

542 [30] C. S. M. Helker *et al.*, “A whole organism small molecule screen identifies novel regulators of
543 pancreatic endocrine development,” *Dev.*, vol. 146, no. 14, 2019, doi: 10.1242/dev.172569.

544 [31] C. Carril Pardo *et al.*, “A delta-cell subpopulation with a pro-beta-cell identity contributes to
545 efficient age-independent recovery in a zebrafish model of diabetes,” *Elife*, 2022.

546 [32] S. P. Singh *et al.*, “A single-cell atlas of de novo β-cell regeneration reveals the contribution of
547 hybrid β/δ-cells to diabetes recovery in zebrafish,” *Development*, vol. 149, no. 2, 2022, doi:
548 10.1242/dev.199853.

549 [33] N. Ninov, D. Hesselson, P. Gut, A. Zhou, K. Fidelin, and D. Y. R. Stainier, “Metabolic regulation
550 of cellular plasticity in the pancreas,” *Curr. Biol.*, vol. 23, no. 13, pp. 1242–1250, 2013, doi:
551 10.1016/j.cub.2013.05.037.

552 [34] M. J. Parsons *et al.*, “Notch-responsive cells initiate the secondary transition in larval zebrafish
553 pancreas,” *Mech. Dev.*, vol. 126, no. 10, pp. 898–912, 2009, doi: 10.1016/j.mod.2009.07.002.

554 [35] N. Ninov, M. Borius, and D. Y. R. Stainier, “Different levels of Notch signaling regulate
555 quiescence, renewal and differentiation in pancreatic endocrine progenitors,” *Development*,
556 vol. 139, no. 9, pp. 1557–1567, 2012, doi: 10.1242/dev.076000.

557 [36] V. A. Tornini *et al.*, “Live Monitoring of Blastemal Cell Contributions During Appendage
558 Regeneration,” *Curr. Biol.*, 2016, doi: 10.1016/j.cub.2016.08.072.Live.

559 [37] S. C. McMillan *et al.*, “A regulatory pathway involving retinoic acid and calcineurin demarcates
560 and maintains joint cells and osteoblasts in regenerating fin,” *Dev.*, vol. 145, no. 11, 2018, doi:
561 10.1242/DEV.161158.

562 [38] Z. Cao *et al.*, “Calcineurin controls proximodistal blastema polarity in zebrafish fin
563 regeneration,” *Proc. Natl. Acad. Sci. U. S. A.*, vol. 118, no. 2, pp. 2–9, 2021, doi:
564 10.1073/pnas.2009539118.

565 [39] S. Kujawski *et al.*, “Calcineurin Regulates Coordinated Outgrowth of Zebrafish Regenerating
566 Fins,” *Dev. Cell*, vol. 28, no. 5, pp. 573–587, 2014, doi: 10.1016/j.devcel.2014.01.019.

567 [40] E. Tarifeño-Saldivia *et al.*, “Transcriptome analysis of pancreatic cells across distant species
568 highlights novel important regulator genes,” *BMC Biol.*, vol. 15, no. 1, pp. 1–19, 2017, doi:
569 10.1186/s12915-017-0362-x.

570 [41] J. J. Heit *et al.*, “Calcineurin/NFAT signalling regulates pancreatic β-cell growth and function,”
571 *Nature*, vol. 443, no. 7109, pp. 345–349, 2006, doi: 10.1038/nature05097.

572 [42] J. Lu *et al.*, “ IGFBP 1 increases β-cell regeneration by promoting α- to β-cell
573 transdifferentiation ,” *EMBO J.*, vol. 35, no. 18, pp. 2026–2044, 2016, doi:
574 10.15252/embj.201592903.

575 [43] C. Karampelias *et al.*, “Reinforcing one-carbon metabolism via folic acid/Folr1 promotes β-cell
576 differentiation,” *Nat. Commun.*, vol. 12, no. 1, pp. 1–13, 2021, doi: 10.1038/s41467-021-
577 23673-0.

578 [44] K. C. Liu *et al.*, “Inhibition of Cdk5 promotes β-cell differentiation from ductal progenitors,”
579 *Diabetes*, vol. 67, no. 1, pp. 58–70, 2017, doi: 10.2337/db16-1587.

580 [45] X. Wu *et al.*, “Calcineurin and ATF3: opposite roles in squamous skin cancer,” *Nature*, 2010,
581 doi: 10.1038/nature08996.Calcineurin.

582 [46] C. Mammucari *et al.*, “Integration of notch 1 and calcineurin/NFAT signaling pathways in
583 keratinocyte growth and differentiation control,” *Dev. Cell*, vol. 8, no. 5, pp. 665–676, 2005,
584 doi: 10.1016/j.devcel.2005.02.016.

585 [47] Y. H. Kim, H. L. Larsen, P. Rué, L. A. Lemaire, J. Ferrer, and A. Grapin-Botton, “Cell Cycle–
586 Dependent Differentiation Dynamics Balances Growth and Endocrine Differentiation in the
587 Pancreas,” *PLoS Biol.*, vol. 13, no. 3, 2015, doi: 10.1371/journal.pbio.1002111.

588 [48] N. A. J. Krentz *et al.*, “Phosphorylation of NEUROG3 Links Endocrine Differentiation to the Cell
589 Cycle in Pancreatic Article Phosphorylation of NEUROG3 Links Endocrine Differentiation to the
590 Cell Cycle in Pancreatic Progenitors,” *Dev. Cell*, vol. 41, no. 2, pp. 129-142.e6, 2017, doi:
591 10.1016/j.devcel.2017.02.006.

592 [49] L. C. Flasse, D. G. Stern, J. L. Pirson, I. Manfroid, B. Peers, and M. L. Voz, “The bHLH
593 transcription factor Ascl1a is essential for the specification of the intestinal secretory cells and
594 mediates Notch signaling in the zebrafish intestine,” *Dev. Biol.*, vol. 376, no. 2, pp. 187–197,
595 2013, doi: 10.1016/j.ydbio.2013.01.011.

596 [50] W. B. Huttner and Y. Kosodo, “Symmetric versus asymmetric cell division during neurogenesis
597 in the developing vertebrate central nervous system,” *Curr. Opin. Cell Biol.*, vol. 17, no. 6, pp.

598 648–657, 2005, doi: 10.1016/j.ceb.2005.10.005.

599 [51] A. D. Ho and W. Wagner, “The beauty of asymmetry: Asymmetric divisions and self-renewal in
600 the haematopoietic system,” *Curr. Opin. Hematol.*, vol. 14, no. 4, pp. 330–336, 2007, doi:
601 10.1097/MOH.0b013e3281900f12.

602 [52] R. S. Bultje, D. R. Castaneda-Castellanos, L. Y. Jan, Y. N. Jan, A. R. Kriegstein, and S. H. Shi,
603 “Mammalian Par3 Regulates Progenitor Cell Asymmetric Division via Notch Signaling in the
604 Developing Neocortex,” *Neuron*, vol. 63, no. 2, pp. 189–202, 2009, doi:
605 10.1016/j.neuron.2009.07.004.

606 [53] M. Guo, L. Y. Jan, and Y. N. Jan, “Control of daughter cell fates during asymmetric division:
607 Interaction of Numb and Notch,” *Neuron*, vol. 17, no. 1, pp. 27–41, 1996, doi: 10.1016/S0896-
608 6273(00)80278-0.

609 [54] K. Sousounis *et al.*, “Eya2 promotes cell cycle progression by regulating DNA damage response
610 during vertebrate limb regeneration,” 2020.

611 [55] S. Da *et al.*, “Cell senescence contributes to tissue regeneration in zebrafish,” no. July 2019,
612 pp. 1–5, 2020, doi: 10.1111/acel.13052.

613 [56] A. S. Md Moin, P. C. Butler, and A. E. Butler, “Increased proliferation of the pancreatic duct
614 gland compartment in type 1 diabetes,” *J. Clin. Endocrinol. Metab.*, vol. 102, no. 1, pp. 200–
615 209, 2017, doi: 10.1210/jc.2016-3001.

616 [57] A. P. Ghaye *et al.*, “Progenitor potential of nkx6.1-expressing cells throughout zebrafish life
617 and during beta cell regeneration,” *BMC Biol.*, vol. 13, no. 1, 2015, doi: 10.1186/s12915-015-
618 0179-4.

619 [58] D. Bergemann *et al.*, “Nifurpirinol: A more potent and reliable substrate compared to
620 metronidazole for nitroreductase-mediated cell ablations,” *Wound Repair Regen.*, vol. 26, no.
621 2, pp. 238–244, 2018, doi: 10.1111/wrr.12633.

622 [59] K. M. Kwan *et al.*, “The Tol2kit: a multisite gateway-based construction kit for Tol2 transposon
623 transgenesis constructs.,” *Dev. Dyn. an Off. Publ. Am. Assoc. Anat.*, vol. 236, no. 11, pp.
624 3088–3099, Nov. 2007, doi: 10.1002/dvdy.21343.

625 [60] K. Kawakami, “Tol2: a versatile gene transfer vector in vertebrates.,” *Genome Biol.*, vol. 8
626 Suppl 1, p. S7, 2007, doi: 10.1186/gb-2007-8-s1-s7.

627

628 **Legends**

629

630 **Figure 1 :** *Transcriptomic profiling of ductal cells during beta cell regeneration and validation in larvae*

631 A-B) Enrichment ratio of selected non-redundant signatures of KEGG pathways overrepresented
632 in ductal cells after beta cells ablation (UP – A and DOWN -B) compared to ductal cells without
633 beta cells ablation. Gene Ontology (GO) terms were identified using ORA analysis by WebGestalt
634 (Liao et al., 2019) using the list of DE genes provided by DESeq. The light color for Notch pathway
635 means p-value = 0.11.

636 C) List of genes associated with the signature of cellular senescence from A-B. Genes related to
637 CaN pathway are in bold.

638 D) Calcineurin canonical pathway with genes in green that are modulated in transcriptomic data
639 from A-B.

640 E) Experimental design for regeneration test in larvae. Briefly, after nifurpirinol treatment from 3
641 to 4dpf, larvae were fixed and analyzed at 4-7-10 and 14 days post treatment (dpt).

642 F) Graph representing the mean number of mCherry+ beta cells in the pancreatic tail of *Tg(ins:NTR-*
643 *P2A-mCherry) ; Tg(nkx6.1:GFP)* at 0-4-7-10 and 14 dpt. The gray spheres represent non-ablated
644 conditions and the pink triangles the ablated condition. Data are presented as mean values ± SEM.
645 One-way ANOVA test with Tukey's multiple comparison test, ****p-value>0.0005.

646 G) Whole mount fluorescent immunohistochemistry (GFP and mCherry) of the pancreas of
647 *Tg(ins:NTR-P2A-mCherry) ; Tg(nkx6.1:GFP)* larvae at 14dpt. 3D projection (stack) of one non-
648 ablated and one ablated representative samples. The principal islet (PI) and the pancreatic tail are
649 shown. Arrows point out mCherry+ beta cells in the pancreatic tail. Scale 100µM.

650 H) Experimental design for EdU assay in larvae. After NFP treatment for 3 to 4dpf, larvae were
651 exposed to EdU at 2dpt before fixation for analysis.

652 I) Whole mount fluorescent immunohistochemistry (GFP and EdU) of the pancreatic tail of
653 *Tg(ins:NTR-P2A-mCherry) ; Tg(nkx6.1:GFP)* larvae at 2dpt. 3D projection (stack) of one non-ablated
654 and one ablated representative samples. Arrows point out GFP+ duct cells EdU+ in the pancreatic
655 tail. Scale 50µM.

656 J) Barplot representing the percentage of GFP+ ductal cells which incorporated EdU+ in non-
657 ablated and ablated conditions. Data are presented as mean values ± SD. T-test. **p-value>0.005.

658

659 **Figure 2 :** *Calcineurin inhibition with CsA increases the ductal regenerative response*

660 **A)** Experimental design for regeneration test in larvae with CsA treatment. Briefly, after
661 nifurpirinol treatment from 3 to 4dpf, larvae were treated with CsA from 1 to 3dpt and fixed
662 and analyzed at 4-7-10 and 14 days post treatment (dpt).
663 **B)** Graph representing the mean number of mCherry+ beta cells in the pancreatic tail of
664 *Tg(ins:NTR-P2A-mCherry) ; Tg(nkx6.1:GFP)* at 0-4-7-10 and 14 dpt. The gray spheres represent
665 non-ablated condition ; the pink triangles represent the ablated condition ; the black squares
666 CsA condition and inverted green triangles ablated + CsA condition. Data are presented as

667 mean values ± SEM. Two-way ANOVA test with Sidak's multiple comparisons test, *p-
668 value>0.05.
669 **C)** Whole mount fluorescent immunohistochemistry (GFP and mCherry) of the pancreas of
670 *Tg(ins:NTR-P2A-mCherry) ; Tg(nkx6.1:GFP)* larvae at 10dpt. 3D projection (stack) of non-
671 ablated and ablated larvae treated with DMSO or CsA representative samples. The principal
672 islet (PI) and the pancreatic tail are shown. Arrows point out mCherry+ beta cells in the
673 pancreatic tail. Scale 100µM.
674 **D)** Barplot representing the number of number of mCherry+ beta cells in the pancreatic tail of
675 *Tg(ins:NTR-P2A-mCherry) ; Tg(nkx6.1:GFP)* larvae at 10dpt. The gray spheres represent non-
676 ablated condition ; the pink triangles represent the ablated condition ; the black squares CsA
677 condition and inverted green triangles ablated + CsA condition. Data are presented as mean
678 values ± SD. Two-way ANOVA with Tukey's multiple comparison test, *p-value>0.05.
679 **E)** Graph representing the mean number of GFP+ neurod1+ cells in the pancreatic tail of
680 *Tg(ins:NTR-P2A-mCherry) ; Tg(neurod1:GFP)* at 0-4-7 and 10 dpt. The gray spheres represent
681 non-ablated condition ; the pink triangles represent the ablated condition ; the black squares
682 CsA condition and inverted green triangles ablated + CsA condition. Data are presented as
683 mean values ± SEM. Two-way ANOVA test with Sidak's multiple comparisons test, **p-
684 value>0.005; *** p-value>0.0005; **** p-value>0.00005.
685 **F)** Graph representing the mean number of GFP+ neurod1 EdU+ cells in the pancreatic tail of
686 *Tg(ins:NTR-P2A-mCherry) ; Tg(neurod1:GFP)* at 0-4-7 and 10 dpt. The gray spheres represent
687 non-ablated condition ; the pink triangles represent the ablated condition ; the black squares
688 CsA condition and inverted green triangles ablated + CsA condition. Data are presented as
689 mean values ± SEM.
690
691
692 **Figure 3:** *Transgenic mediated overexpression of calcineurin abolish the ductal regenerative response*
693
694 **A)** Experimental design for regeneration test in larvae with heat-shocks. Briefly, after nifurpirinol
695 treatment from 3 to 4dpf, four heat shock were performed from 1 to 3dpt and larvae were
696 fixed and analyzed at 14dpt.
697 **B)** Whole mount fluorescent immunohistochemistry (GFP and mCherry) of the pancreas of
698 *Tg(hsp70:CaN^{CA})*; *Tg(ins:NTR-P2A-mCherry); Tg(nkx6.1:GFP)* larvae at 14dpt. 3D projection
699 (stack) of one non-ablated and one ablated with or without heat-shock representative
700 samples. The principal islet (PI) and the pancreatic tail are showed. Arrows point out mCherry+
701 beta cells in the pancreatic tail. Scale 100µM.
702 **C)** Barplot representing the mean number of mCherry+ beta cells in the pancreatic tail of
703 *Tg(hsp70:CaN^{CA})*; *Tg(ins:NTR-P2A-mCherry); Tg(nkx6.1:GFP)* larvae at 14dpt. The gray spheres
704 represent non-ablated condition ; the pink triangles represent the ablated condition ; the black
705 squares heat-shock condition and inverted green triangles ablated + heat-shock condition.
706 Data are presented as mean values ± SD. Two-way ANOVA with Tukey's multiple comparisons
707 test, *p-value>0.05, *** p-value>0.0005, ns = non-significant.
708 **D)** Whole mount fluorescent immunohistochemistry (GFP and mCherry) of the pancreas of larvae
709 at 14dpt. 3D projection (stack) of *Tg(ins:NTR-P2A-mCherry) ; Tg(nkx6.1:GFP)* one non-ablated
710 and one ablated representative control samples and *Tg(UAS:CaN^{CA})*; *Tg(ins:NTR-P2A-mCherry)*
711 *; Tg(cftr:gal4)* one non-ablated and one ablated representative samples. The principal islet (PI)
712 and the pancreatic tail are showed. Arrows point out mCherry+ beta cells in the pancreatic tail.
713 Scale 100µM.

714 **E)** Barplot representing the mean number of mCherry+ beta cells in the pancreatic tail of larvae
715 at 14dpt. The gray spheres represent non-ablated *Tg(ins:NTR-P2A-mCherry) ; Tg(nkx6.1:GFP)*
716 condition ; the pink triangles represent the ablated *Tg(ins:NTR-P2A-mCherry) ; Tg(nkx6.1:GFP)*
717 condition ; the black squares non-ablated *Tg(UAS:CaN^{CA})*; *Tg(ins:NTR-P2A-mCherry) ;*
718 *Tg(cftr:gal4)* condition and inverted green triangles ablated *Tg(UAS:CaN^{CA})*; *Tg(ins:NTR-P2A-*
719 *mCherry) ; Tg(cftr:gal4)* condition. Data are presented as mean values ± SD. Two-way ANOVA
720 with Tukey's multiple comparison test, *** means p-value>0.0005, **** p-value>0.00005, ns
721 = non-significant.

722 **Figure 4:** *CaN repression potentializes the effect of Notch inhibition on beta cell formation*

723 **A)** Experimental design for Notch inhibition test in non-ablated condition. Larvae were treated
724 concomitantly with LY411575 (Notch inhibitor) and CsA from 3 to 4dpf and were fixed and
725 analyzed at 6dpf.
726 **B)** Graph representing the mean number of mCherry+ beta cells in the pancreatic tail of
727 *Tg(ins:NTR-P2A-mCherry) ; Tg(nkx6.1:GFP)* larvae at 6 dpf depending the concentration of
728 LY411575. The blue dots represent LY411575; and purple combination of LY411575 and CsA.
729 Data are presented as mean values ± SEM. Two-way ANOVA test with Sidak's multiple
730 comparison test, *p-value>0.05, **p-value>0.05, ns = non-significant.
731 **C)** Whole mount fluorescent immunohistochemistry (GFP and mCherry) of the pancreas of
732 *Tg(ins:NTR-P2A-mCherry) ; Tg(nkx6.1:GFP)* larvae at 6dpf. 3D projection (stack) of one control
733 (without any treatment) ; one CsA-treated ; one LY411757-treated and one with both CsA and
734 LY411575 treated larvae. The principal islet (PI) and the pancreatic tail are showed. Arrows
735 point out mCherry+ beta cells in the pancreatic tail. Scale 50µM.
736 **D)** Barplot representing the mean number of mCherry+ beta cells in the pancreatic tail of
737 *Tg(ins:NTR-P2A-mCherry) ; Tg(nkx6.1:GFP)* larvae at 6dpf. The black dots represent the
738 control; gray CsA treatment ;blue LY411575; and purple combination of LY411575 and CsA.
739 Data are presented as mean values ± SD. Two-way ANOVA with Tukey multiple comparison
740 test, ***p-value>0.0005, ****p-value>0.00005.
741 **E)** Graph representing the mean number of mCherry+ beta cells in the pancreatic tail of
742 *Tg(ins:NTR-P2A-mCherry) ; Tg(nkx6.1:GFP)* larvae at 5-6-7 dpf. The black dots represent the
743 control; gray CsA treatment ;blue LY411575; and purple combination of LY411575 and CsA.
744 Data are presented as mean values ± SEM. Two-way ANOVA test with Sidak's multiple
745 comparison test, *p-value>0.05.

746 **Figure 5:** *CaN repression increases the proportion of duct proliferating cells*

747 **A)** Experimental design for EdU assay in Notch test. Larvae were treated concomitantly with
748 LY411575 (Notch inhibitor) and CsA from 3 to 4dpf and then briefly treated with EdU before
749 fixation and analysis at 4 dpf or at 6dpf.
750 **B)** Whole mount fluorescent immunohistochemistry (GFP and EdU) of the pancreatic tail of
751 *Tg(ins:NTR-P2A-mCherry) ; Tg(nkx6.1:GFP)* larvae at 4dpf. 3D projection (stack) of one control
752 (without any treatment), one with CsA only, one with LY411575 only and one with both CsA
753 and LY411757 representative samples. Scale 50µM.
754 **C)** Barplot representing the percentage of GFP+ ductal cells which incorporated EdU+ in
755 pancreatic tail of *Tg(ins:NTR-P2A-mCherry) ; Tg(nkx6.1:GFP)* larvae for the Notch test. The
756 black dots represent the control; gray CsA treatment ;blue LY411575; and purple combination
757 of LY411575 and CsA. Data are presented as mean values ± SD. T-test. Two-way ANOVA test
758 with Tukey's multiple comparisons test, *p-value>0.05 ; ****p-value>0.00005 ; ns = non-
759 significant.

760 **D)** Barplot representing the number of GFP+ ductal cells which in pancreatic tail of *Tg(ins:NTR-*
761 *P2A-mCherry) ; Tg(nkx6.1:GFP)* larvae at 6dpf for the Notch test. The black dots represent the
762 control; gray CsA treatment ;blue LY411575; and purple combination of LY411575 and CsA.
763 Data are presented as mean values ± SD. T-test. Two-way ANOVA test with Tukey's multiple
764 comparisons test, *p-value>0.05 ; ****p-value>0.00005 ; ns = non-significant.
765 **E)** Experimental design for EdU assay in regeneration. Larvae were treated with nifurpirinol for
766 beta cell ablation from 3 to 4dpf then with CsA from 4 to 5dpf and then briefly treated with
767 EdU before fixation and analysis.
768 **F)** Whole mount fluorescent immunohistochemistry (GFP and EdU) of the pancreatic tail of
769 *Tg(ins:NTR-P2A-mCherry) ; Tg(nkx6.1:GFP)* larvae at 5dpf. 3D projection (stack) of one
770 representative sample of non-ablated or ablated with or without CsA are shown. Scale 50µM.
771 **G)** Barplot representing the percentage of GFP+ ductal cells which incorporated EdU+ in
772 pancreatic tail of *Tg(ins:NTR-P2A-mCherry) ; Tg(nkx6.1:GFP)* larvae at 5dpf. The gray spheres
773 represent non-ablated condition ; the pink triangles the ablated condition ; the black squares
774 CsA condition and inverted green triangles ablated + CsA condition. Data are presented as
775 mean values ± SD. Two-way ANOVA test with Tukey's multiple comparisons test, *p-
776 value>0.05 ; ****p-value>0.00005 ; ns = non-significant.
777 **H)** Whole mount fluorescent immunohistochemistry (VenusPest and EdU) of the pancreatic tail
778 of *Tg(ins:NTR-P2A-mCherry) ; Tg(tp1:VenusPest)* larvae at 5dpf. 3D projection (stack) of one
779 representative sample of non-ablated or ablated with or without CsA are shown. Scale 50µM.
780 **I)** Barplot representing the percentage of GFP+ ductal cells which incorporated EdU+ in
781 pancreatic tail of *Tg(ins:NTR-P2A-mCherry) ; Tg(tp1:VenusPest)* larvae at 5dpf. The gray
782 spheres represent non-ablated condition ; the pink triangles the ablated condition ; the black
783 squares CsA condition and inverted green triangles ablated + CsA condition. Data are
784 presented as mean values ± sd. Two-way ANOVA test with Tukey multiple comparisons test,
785 *p-value>0.05 ; ****p-value>0.00005 ; ns means non-significant.
786 **J)** Barplot representing the number of VenusPest+ ductal cells which incorporated EdU+ in
787 pancreatic tail of *Tg(ins:NTR-P2A-mCherry) ; Tg(tp1:VenusPest)* larvae at 5dpf. The gray
788 spheres represent non-ablated condition ; the pink triangles the ablated condition ; the black
789 squares CsA condition and inverted green triangles ablated + CsA condition. Data are
790 presented as mean values ± SD. Two-way ANOVA test with Tukey's multiple comparisons test,
791 **p-value>0.005.
792

793 **Figure 6:** *CaN regulation is important in juveniles/adults and necessary for correct glycemia recovery*

794 **A)** Whole mount fluorescent immunohistochemistry (GFP and mCherry) of the pancreas of
795 *Tg(ins:NTR-P2A-mCherry) ; Tg(nkx6.1:GFP)* 2 months old zebrafish at 7dpt. 3D projection (stack)
796 of non-ablated and ablated larvae treated with DMSO or CsA representative samples. The
797 principal islet (PI) and the pancreatic tail are shown. Arrows point out mCherry+ beta cells in
798 the pancreatic tail. Scale 200µM

799 **B-C)** Barplot representing the number of number of mCherry+ small secondary islets (=<5 cells) in
800 the pancreatic tail of *Tg(ins:NTR-P2A-mCherry) ; Tg(nkx6.1:GFP)* 2 months old zebrafish at 7 **(B)** and
801 10dpt **(C).** The gray spheres represent non-ablated condition ; the pink triangles represent the
802 ablated condition ; the black squares CsA condition and inverted green triangles ablated + CsA
803 condition. Data are presented as mean values ± SD. Two-way ANOVA with Tukey's multiple
804 comparison test, *p-value>0.05.

805

806 **D-E)** Barplot representing the glycemia (mg/dL) of *Tg(ins:NTR-P2A-mCherry) ;* months old adult
807 zebrafish at 7 **(D)** and 10dpt **(E).** The pink triangles represent the ablated condition ; the inverted
808 green triangles ablated + CsA condition; the blue squares *Tg(hsp70:CaN^{CA})* after heat shocks ; the
809 orange lozenges *Tg(UAS:CaN^{CA})*; *Tg(cftr:gal4)*. The grey line represents the mean glycemia of
810 controls (non-ablated) fish. Data are presented as mean values ± SD. One-way ANOVA with Tukey's
811 multiple comparison test, *p-value>0.05; **p-value>0.005.

812

813 **Figure 7:** *Model of CaN action on ductal progenitors to regenerate beta cells*

814 **A)** Under physiological conditions, the behavior of the ductal progenitors is determined by
815 Notch signaling. Calcineurin is active in these progenitors and enable a proper control
816 between proliferation and differentiation. When CaN in repressed, more ductal
817 progenitors enter in the cell cycle (2dpt) and switch to a mode of proliferation leading to
818 differentiation of the two daughter cells (4dpt), as more pro-endocrine cells are formed.
819 The result is a exhaustion of the progenitors and a premature beta cell differentiation
820 (10dpt).

821

822 **Figure 1 supplemental :** *Transcriptomic profiling of ductal cells during beta cell regeneration and*
823 *validation in larvae*

824 A) Expression of *ppp3cca; ppp3ccb ; nfatc3a ; nfatc3b* in acinar, alpha, beta, delta or ductal cells
825 population from the zebrafish pancreas [40].

826 B) Calcineurin (*ppp3ccb and ppp3cca)* and NFATc3 (*nfatc3a and nfatc3b)* expression in ductal cells
827 from zebrafish in non-ablated and ablated conditions.

828 **Figure 2 supplemental :** *Calcineurin inhibition with CsA increases the ductal regenerative response*

829 **A)** Whole mount fluorescent immunohistochemistry (mCherry) of the pancreas of *Tg(ins:NTR-*
830 *P2A-mCherry)* larvae at 4-7 and 14dpt. 3D projection (stack) of ablated larvae treated with
831 DMSO or CsA representative samples. The principal islet (PI) and the pancreatic tail are shown.
832 Scale 50 or 100µM.

833 **B-C)** Barplot representing the number of mCherry+ beta cells in the principal islet (PI) **(B)** and the
834 number of secondary islets of mCherry+ beta cells in the pancreatic tail **(C)** of Tg(ins:NTR-P2A-
835 mCherry) ; Tg(nkx6.1:GFP) larvae at 10dpt. Data are presented as mean values ± SD. T-test or
836 Two-way ANOVA with Tukey's multiple comparison test. **p-value>0.005

837 **D)** Experimental design for EdU assay in larvae. After NFP treatment for 3 to 4dpf, larvae were
838 exposed to EdU before fixation for analysis.

839 **E)** Whole mount fluorescent immunohistochemistry (GFP and EdU) of the pancreas of
840 Tg(ins:NTR-P2A-mCherry) ; Tg(neurod1:GFP) larvae at 2-4-7 and 10 dpt. 3D projection (stack) of
841 non-ablated and ablated larvae treated with DMSO or CsA representative samples. The principal
842 islet (PI) and the pancreatic tail are shown. Scale 50µM.

843 **F-G)** Barplot representing the number of gcg+ alpha cells **(F)**; the number of GFP+ sst1.1 delta
844 cells **(G);** of Tg(*ins:NTR-P2A-mCherry*) ; Tg(*sst1.1:GFP*) larvae at 10dpt. Gcg was detected by IHC.
845 The gray spheres represent non-ablated condition ; the pink triangles represent the ablated

846 condition ; the black squares CsA condition and inverted green triangles ablated + CsA condition.
847 Data are presented as mean values ± SD. Two-way ANOVA with Tukey's multiple comparison
848 test. **p-value>0.005

849

850 **Figure 4 supplemental :** *CaN repression potentializes the effect of Notch inhibition on beta cell*
851 *formation*

852 **A)** Experimental design for Notch inhibition test in non-ablated condition. Larvae were treated
853 concomitantly with LY411575 (Notch inhibitor) and FK506 from 3 to 4dpf and were fixed and
854 analyzed at 5dpf.
855 **B)** Barplot representing the mean number of mCherry+ beta cells in the pancreatic tail of
856 *Tg(ins:NTR-P2A-mCherry) ; Tg(nkx6.1:GFP)* larvae at 5dpf. The black dots represent the control;
857 gray FK506 treatment ;blue LY411575; and purple combination of LY411575 and FK506. Data
858 are presented as mean values ± SD. Two-way ANOVA with Tukey multiple comparison test,
859 *p-value>0.05,**p-value>0.005, ****p-value>0.00005.
860 **C)** Experimental design for Notch inhibition test in non-ablated condition. Larvae were heat-
861 shocked and then directly treated with LY411575 (Notch inhibitor) from 3 to 4dpf and were
862 fixed and analyzed at 6dpf.
863 **D)** Barplot representing the mean number of mCherry+ beta cells in the pancreatic tail of
864 *Tg(hsp70:CaN^{CA})*; *Tg(ins:NTR-P2A-mCherry) ; Tg(nkx6.1:GFP)* larvae at 5dpf. The black dots
865 represent the control; gray heat-shock ;blue LY411575; and purple combination of LY411575
866 and heat-shock. Data are presented as mean values ± SD. Two-way ANOVA with Tukey multiple
867 comparison test, ****p-value>0.00005.
868 **E)** Barplot representing the mean number of mCherry+ beta cells in the pancreatic tail of
869 *Tg(ins:NTR-P2A-mCherry) ; Tg(nkx6.1:GFP)* larvae at 6dpf after Notch inhibition (LY411575),
870 CaN inhibition (CsA) and NFATc inhibition (CHIR99021). Data are presented as mean values ±
871 SD. Two-way ANOVA with Tukey multiple comparison test, *p-value>0.05,**p-value>0.005,
872 ****p-value>0.00005.
873

874 **Figure 5 supplemental:** *CaN repression increases the proportion of duct proliferating cells*

875 **A-B)** Barplot representing the number of GFP+ ductal cells which in pancreatic tail of *Tg(ins:NTR-*
876 *P2A-mCherry) ; Tg(nkx6.1:GFP)* larvae at 4dpf for the Notch test. **(A)** Mild Notch inhibition with
877 LY411575 5µM and **(B)** stronger Notch inhibition with LY411575 15µM. The black dots represent
878 the control; gray CsA treatment ;blue LY411575; and purple combination of LY411575 and CsA.
879 Data are presented as mean values ± SD. T-test. Two-way ANOVA test with Tukey's multiple
880 comparisons test, *p-value>0.05 ; ****p-value>0.00005 ; ns = non-significant.

881 **Figure 6 supplemental:** *CaN regulation is important in juveniles/adults and necessary for correct*
882 *glycemia recovery*

883 A) Barplot representing the glycemia (mg/dL) of *Tg(ins:NTR-P2A-mCherry) ;* months old adult
884 zebrafish at 14dpt**.** The pink triangles represent the ablated condition ; the inverted green
885 triangles ablated + CsA condition; the blue squares *Tg(hsp70:CaN^{CA})* after heat shocks. The grey
886 line represents the mean glycemia of controls (non-ablated) fish. Data are presented as mean
887 values ± SD.
888 B) Barplot representing the glycemia (mg/dL) of *Tg(ins:NTR-P2A-mCherry) ; and Tg(UAS:CaN^{CA})*;
889 *Tg(cftr:gal4)* in non-ablated adult zebrafish. Data are presented as mean values ± SD.

Figure 1

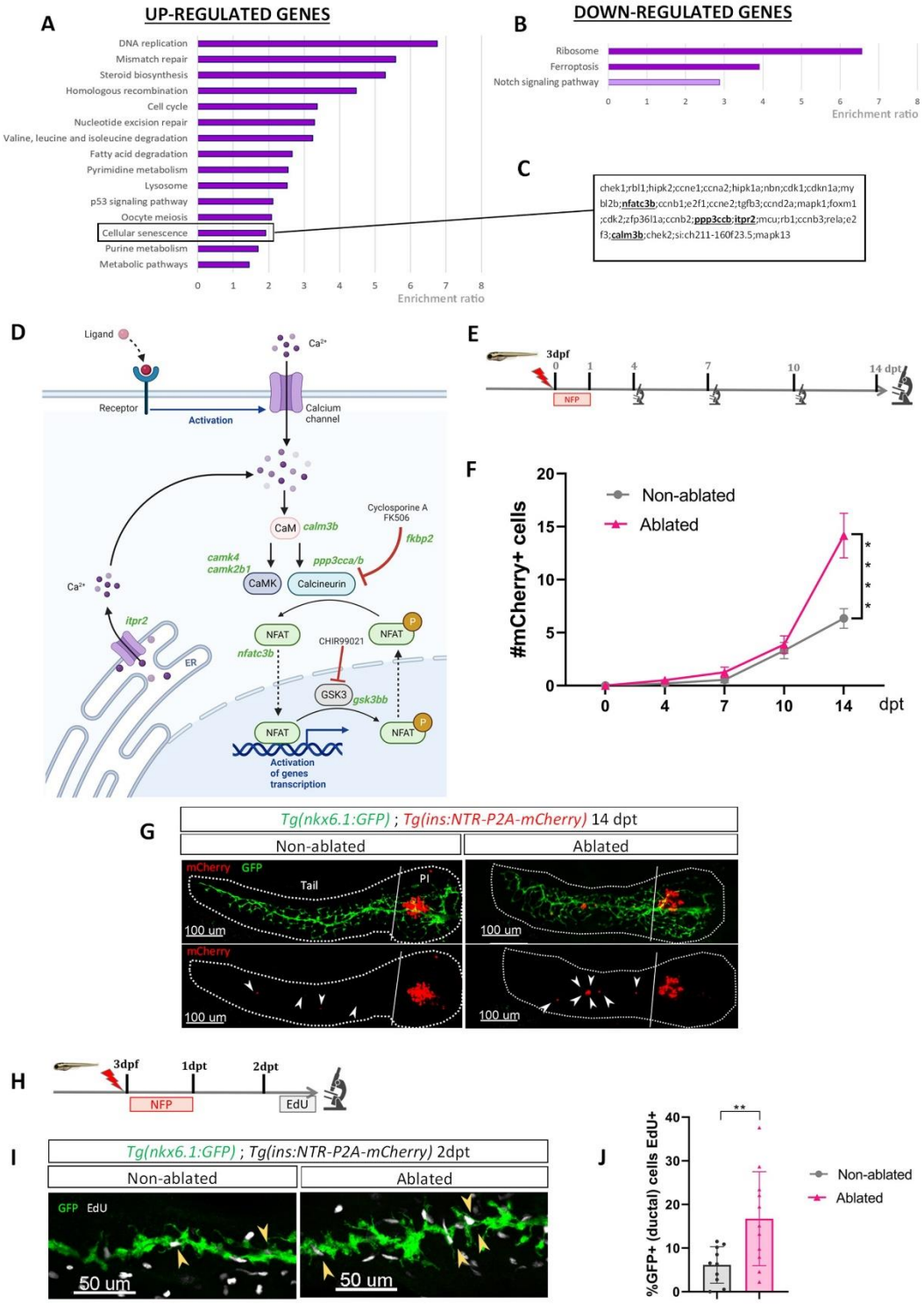
A
UP-REGULATED GENES
DNA replication
Mismatch repair
Steroid biosynthesis
Homologous recombination
Cell cycle
Nucleotide excision repair
Valine, leucine and isoleucine degradation
Fatty acid degradation
Pyrimidine metabolism
Lysosome
p53 signaling pathway
Oocyte meiosis
Cellular senescence
Purine metabolism
Metabolic pathways
Enrichment ratio
B
DOWN-REGULATED GENES
Ribosome
Ferroptosis
Notch signaling pathway
Enrichment ratio
C
chek1;rbl1;hipk2;ccne1;ccna2;hipk1a;nbn;cdk1;cdkn1a;mybl2b;nfatc3b;ccnb1;e2f1;ccne2;tgfb3;ccnd2a;mapk1;foxm1;cdk2;zfp36l1a;ccnb2;ppp3ccb;itpr2;mcu;rb1;ccnb3;rela;e2f3;calm3b;chek2;si:ch211-160f23.5;mapk13
D
Ligand
Receptor
Activation
Calcium channel
CaM
calm3b
Cyclosporine A
FK506
fkbp2
camk4
camk2b1
ppp3cca/b
CaMK
Calcineurin
itpr2
ER
NFAT
nfatc3b
CHIR99021
GSK3
gsk3bb
Activation of genes transcription
E
3dpf
NFP
14 dpt
F
Non-ablated
Ablated
#mCherry+ cells
dpt
G
Tg(nkx6.1:GFP) ; Tg(ins:NTR-P2A-mCherry) 14 dpt
Non-ablated
Ablated
mCherry GFP
Tail
PI
100 um
mCherry
H
3dpf
1dpt
2dpt
NFP
EdU
I
Tg(nkx6.1:GFP) ; Tg(ins:NTR-P2A-mCherry) 2dpt
Non-ablated
Ablated
GFP EdU
50 um
J
%GFP+ (ductal) cells EdU+
Non-ablated
Ablated

890

Figure 2

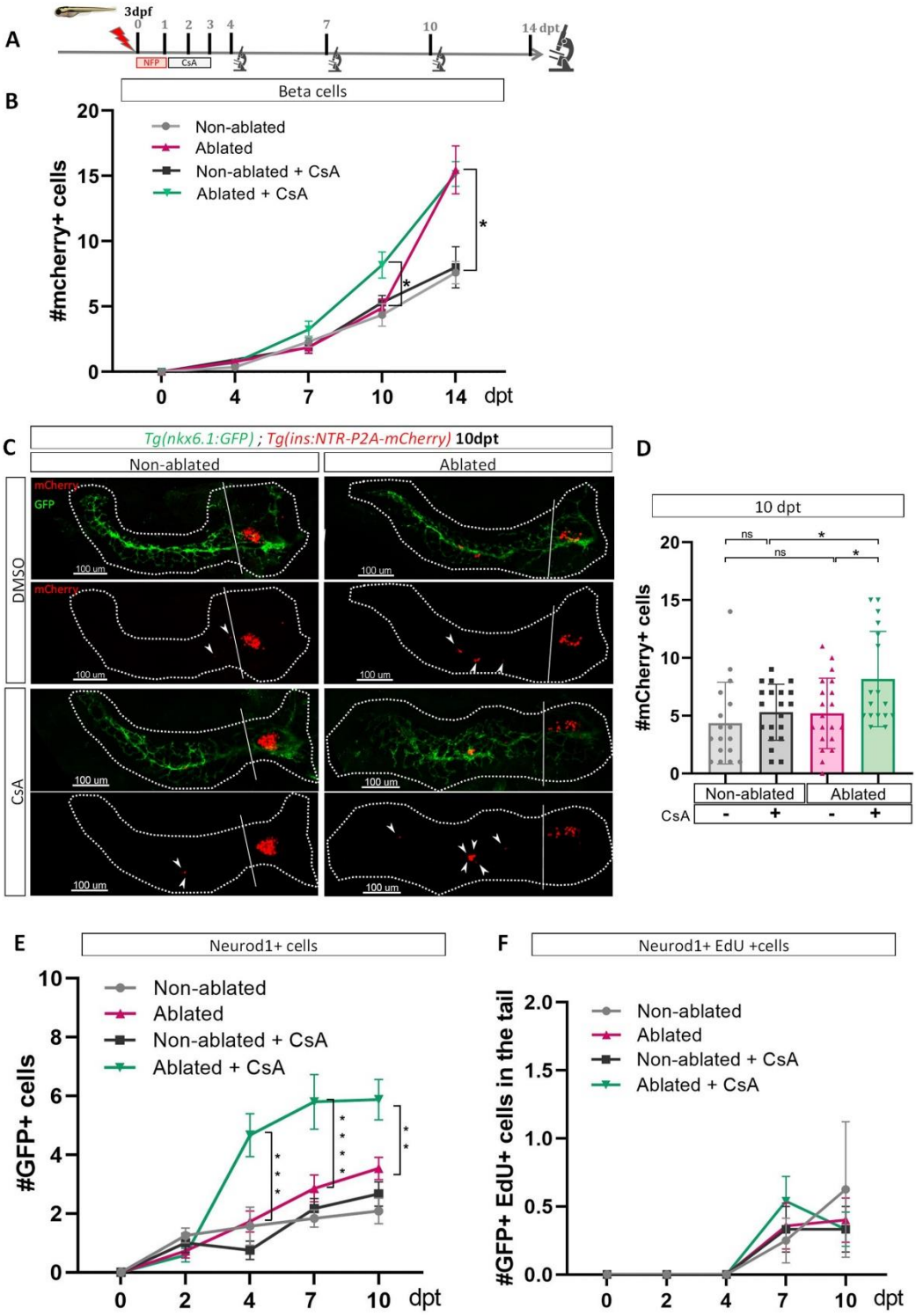
A
3dpf
0 1 2 3 4 7 10 14 dpt
NFP
CsA
B
Beta cells
#mcherry+ cells
Non-ablated
Ablated
Non-ablated + CsA
Ablated + CsA
0 4 7 10 14 dpt
C
Tg(nkx6.1:GFP) ; Tg(ins:NTR-P2A-mCherry) 10dpt
Non-ablated
Ablated
DMSO
CsA
mCherry
GFP
100 um
D
10 dpt
#mCherry+ cells
ns
*
Non-ablated
Ablated
CsA
E
Neurod1+ cells
#GFP+ cells
0 2 4 7 10 dpt
F
Neurod1+ EdU +cells
#GFP+ EdU+ cells in the tail
0 2 4 7 10 dpt

891

Figure 3

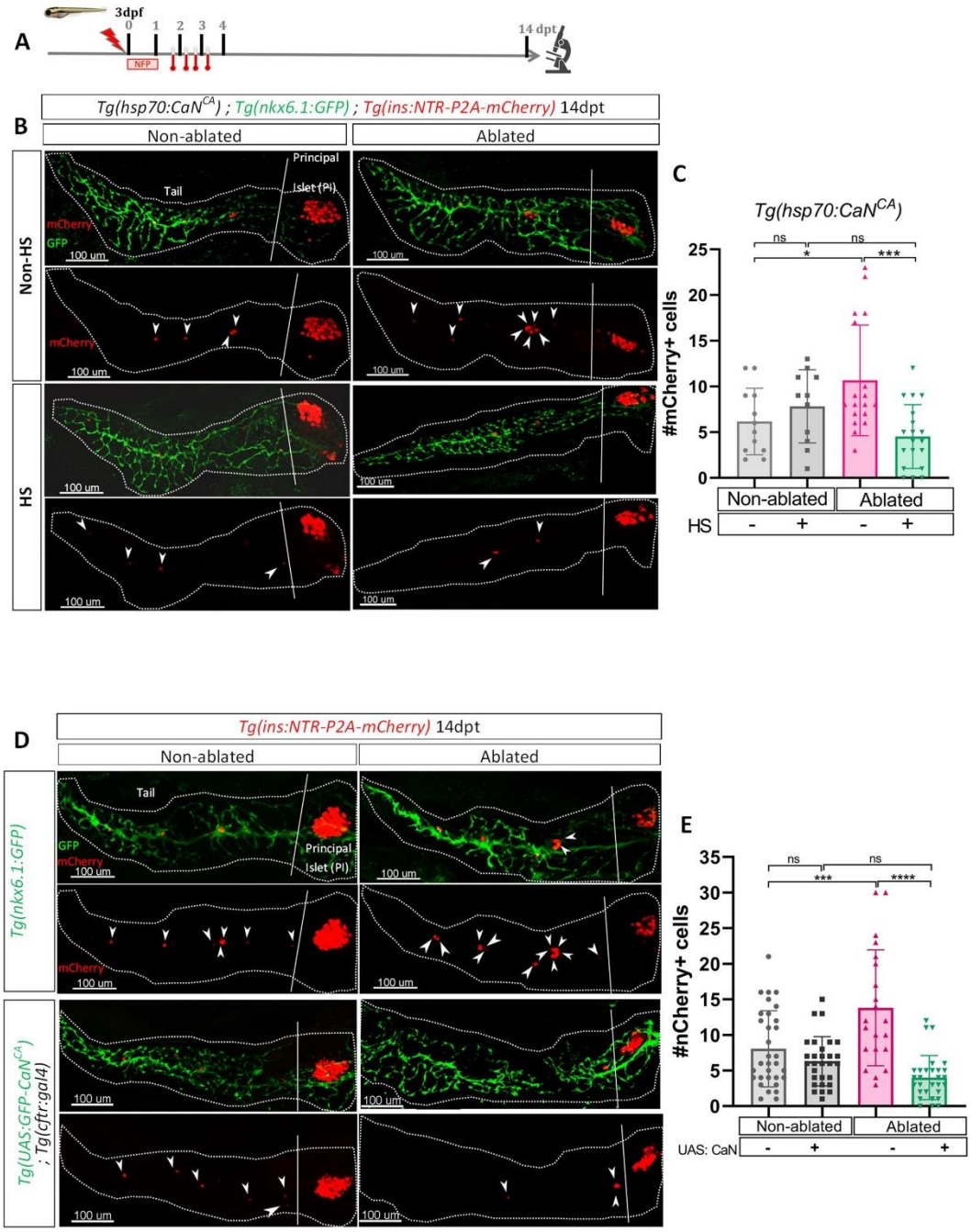
A
3dpf
0 1 2 3 4
NFP
14 dpt
B
Tg(hsp70:CaN^CA) ; Tg(nkx6.1:GFP) ; Tg(ins:NTR-P2A-mCherry) 14dpt
Non-ablated
Ablated
Non-HS
HS
Tail
Principal Islet (PI)
mCherry
GFP
100 um
C
Tg(hsp70:CaN^CA)
#mCherry+ cells
ns
ns
*
***
Non-ablated
Ablated
HS
- + - +
D
Tg(ins:NTR-P2A-mCherry) 14dpt
Non-ablated
Ablated
Tg(nkx6.1:GFP)
Tg(UAS:GFP-CaN^CA) ; Tg(cftr:gal4)
Tail
GFP
mCherry
Principal Islet (PI)
100 um
E
#nCherry+ cells
ns
ns
***
****
Non-ablated
Ablated
UAS: CaN
- + - +

892

Figure 4

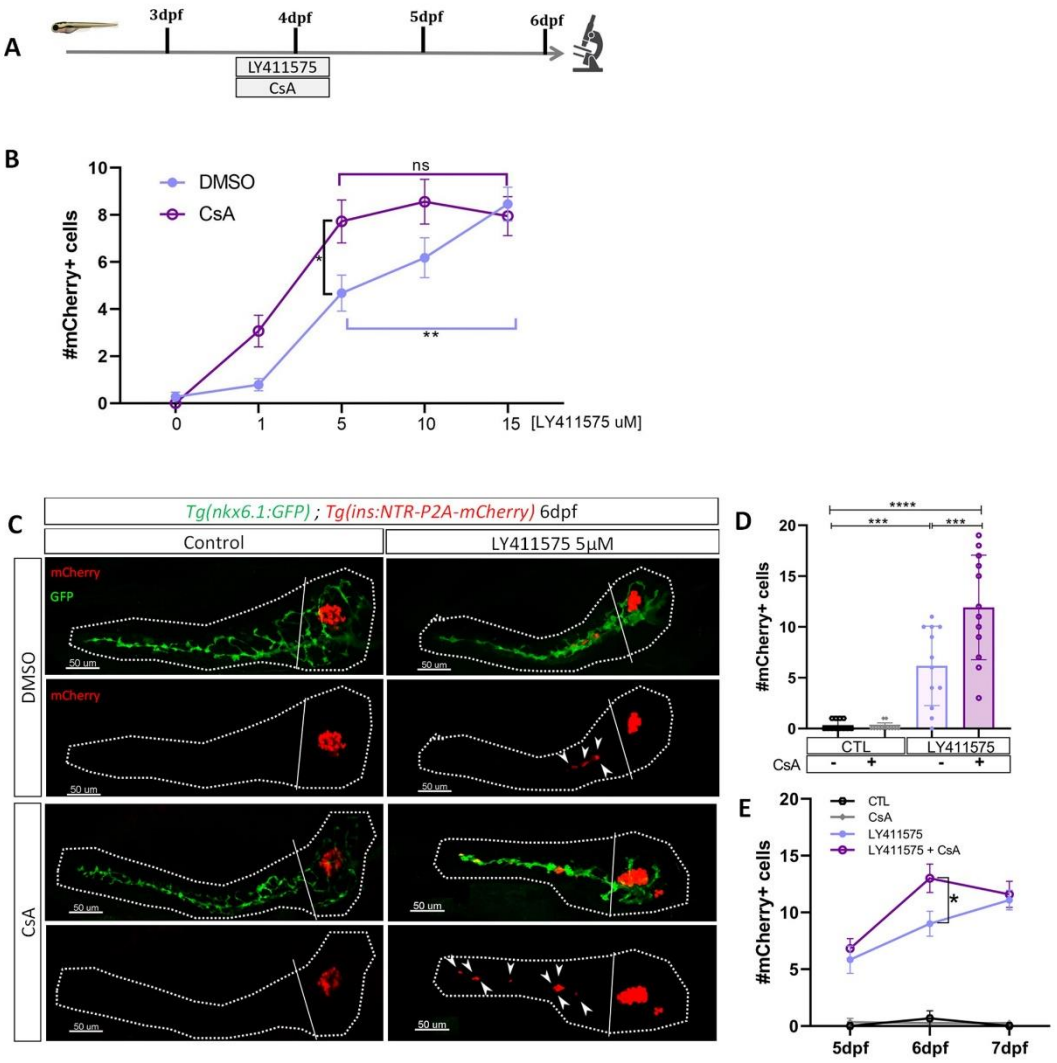
A
3dpf
4dpf
5dpf
6dpf
LY411575
CsA
B
DMSO
CsA
ns
*
**
#mCherry+ cells
[LY411575 uM]
C
Tg(nkx6.1:GFP) ; Tg(ins:NTR-P2A-mCherry) 6dpf
Control
LY411575 5µM
DMSO
CsA
mCherry
GFP
50 um
D
****
***
#mCherry+ cells
CTL
LY411575
CsA
E
CTL
CsA
LY411575
LY411575 + CsA
#mCherry+ cells
5dpf
6dpf
7dpf

893

Figure 5

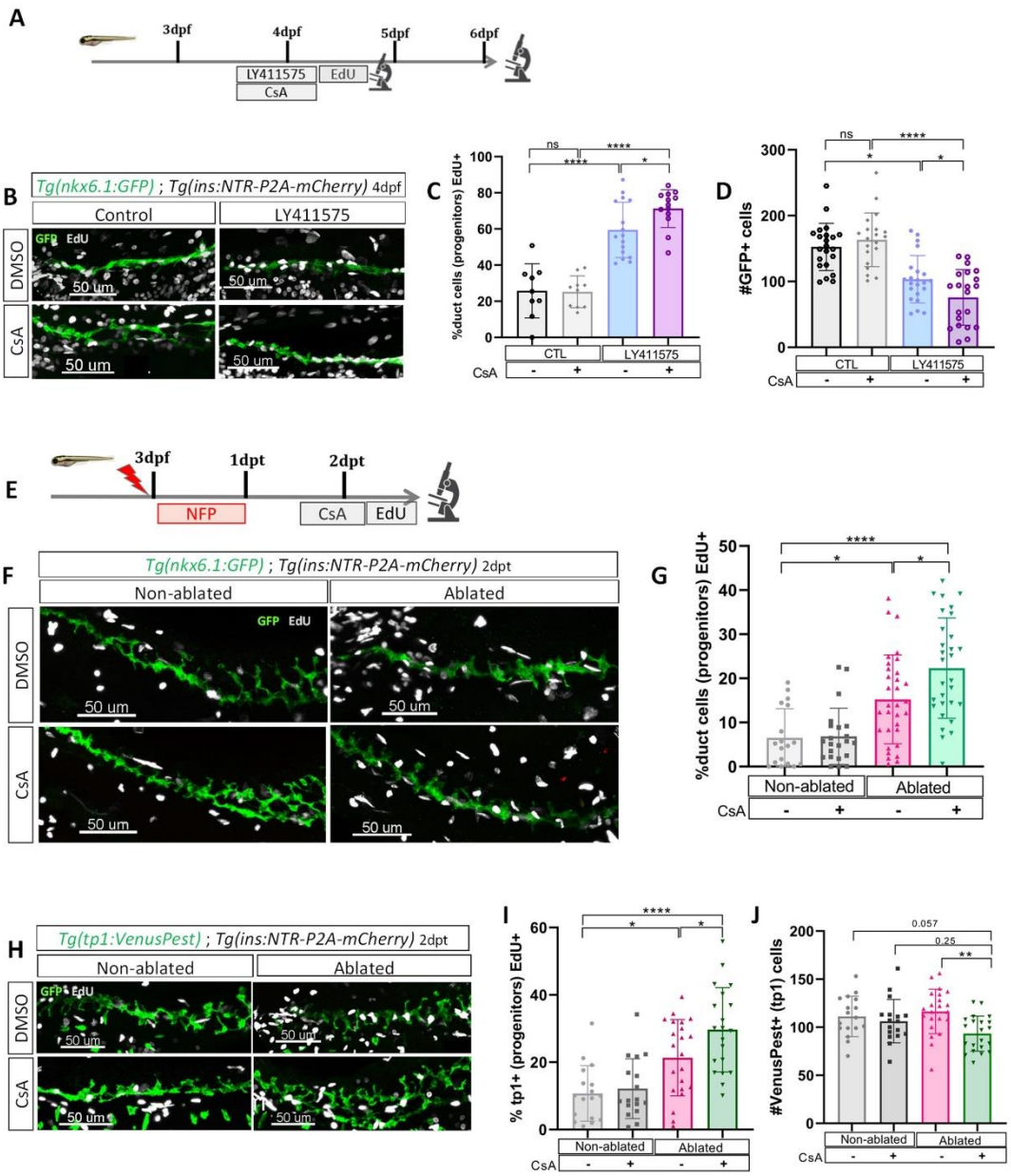
A
3dpf
4dpf
5dpf
6dpf
LY411575
EdU
CsA
B
Tg(nkx6.1:GFP) ; Tg(ins:NTR-P2A-mCherry) 4dpf
Control
LY411575
DMSO
CsA
GFP EdU
50 um
C
%duct cells (progenitors) EdU+
ns
****
*
CTL
LY411575
CsA
D
#GFP+ cells
E
3dpf
1dpt
2dpt
NFP
CsA
EdU
F
Tg(nkx6.1:GFP) ; Tg(ins:NTR-P2A-mCherry) 2dpt
Non-ablated
Ablated
G
%duct cells (progenitors) EdU+
H
Tg(tp1:VenusPest) ; Tg(ins:NTR-P2A-mCherry) 2dpt
I
% tp1+ (progenitors) EdU+
J
#VenusPest+ (tp1) cells
0.057
0.25
**

894

Figure 6

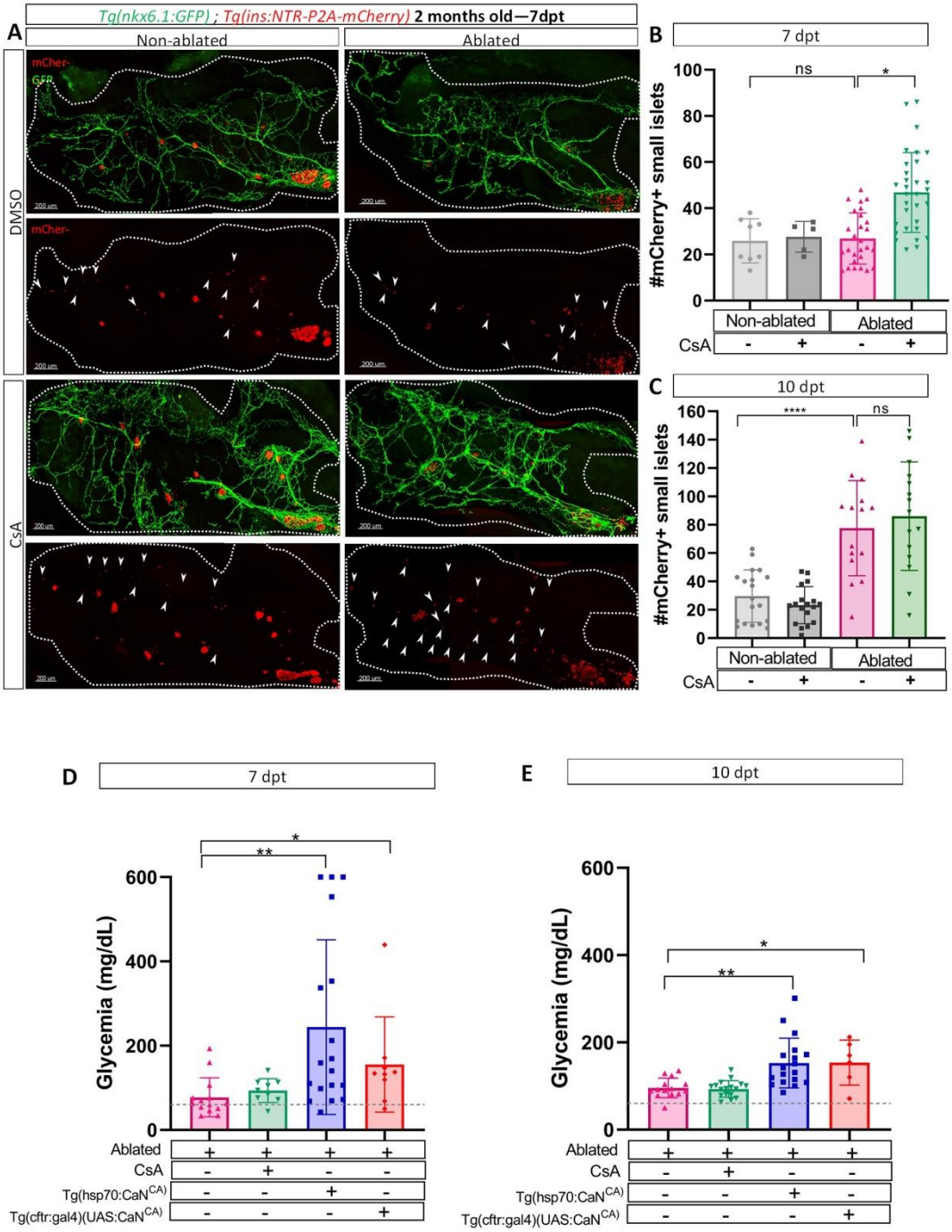
Tg(nkx6.1:GFP) ; Tg(ins:NTR-P2A-mCherry) 2 months old—7dpt
A
Non-ablated
Ablated
DMSO
CsA
mCher-GFP
mCher-
200 um
B
7 dpt
#mCherry+ small islets
ns
*
Non-ablated
Ablated
CsA
C
10 dpt
****
ns
D
7 dpt
Glycemia (mg/dL)
Ablated
CsA
Tg(hsp70:CaN^CA)
Tg(cftr:gal4)(UAS:CaN^CA)
E
10 dpt

Figure 7

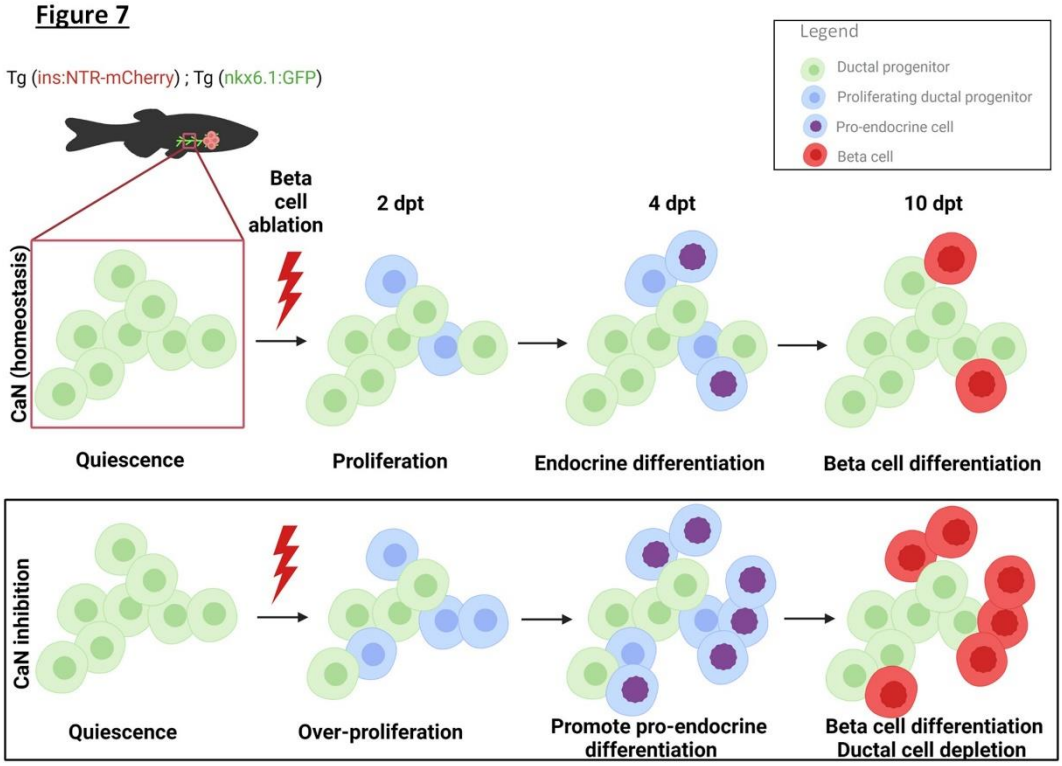
Tg (ins:NTR-mCherry) ; Tg (nkx6.1:GFP)
Legend
Ductal progenitor
Proliferating ductal progenitor
Pro-endocrine cell
Beta cell
Beta cell ablation
2 dpt
4 dpt
10 dpt
CaN (homeostasis)
Quiescence
Proliferation
Endocrine differentiation
Beta cell differentiation
CaN inhibition
Quiescence
Over-proliferation
Promote pro-endocrine differentiation
Beta cell differentiation
Ductal cell depletion

896

Figure 1 supplemental

A

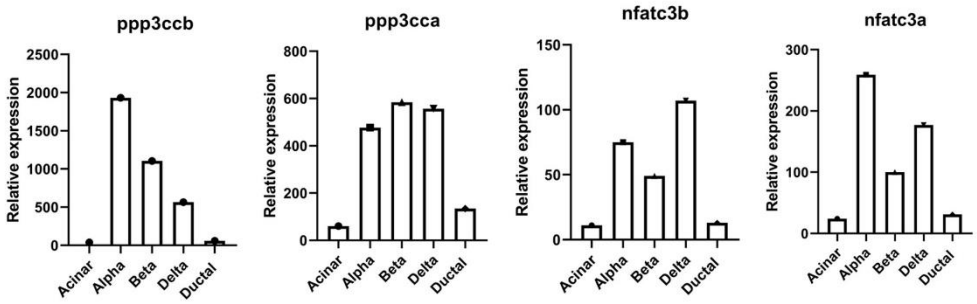

B

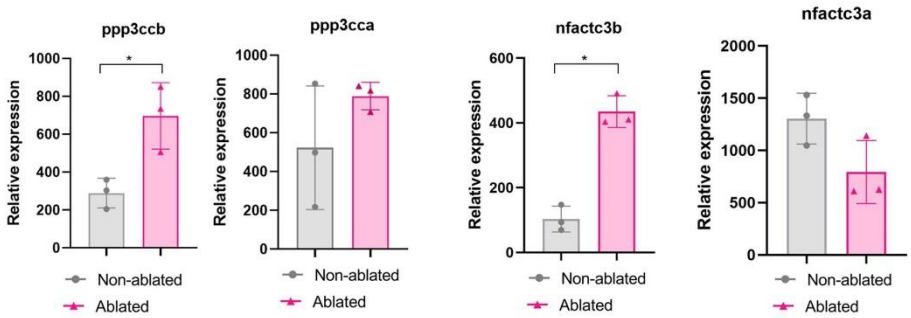

897

Figure 2 supplemental

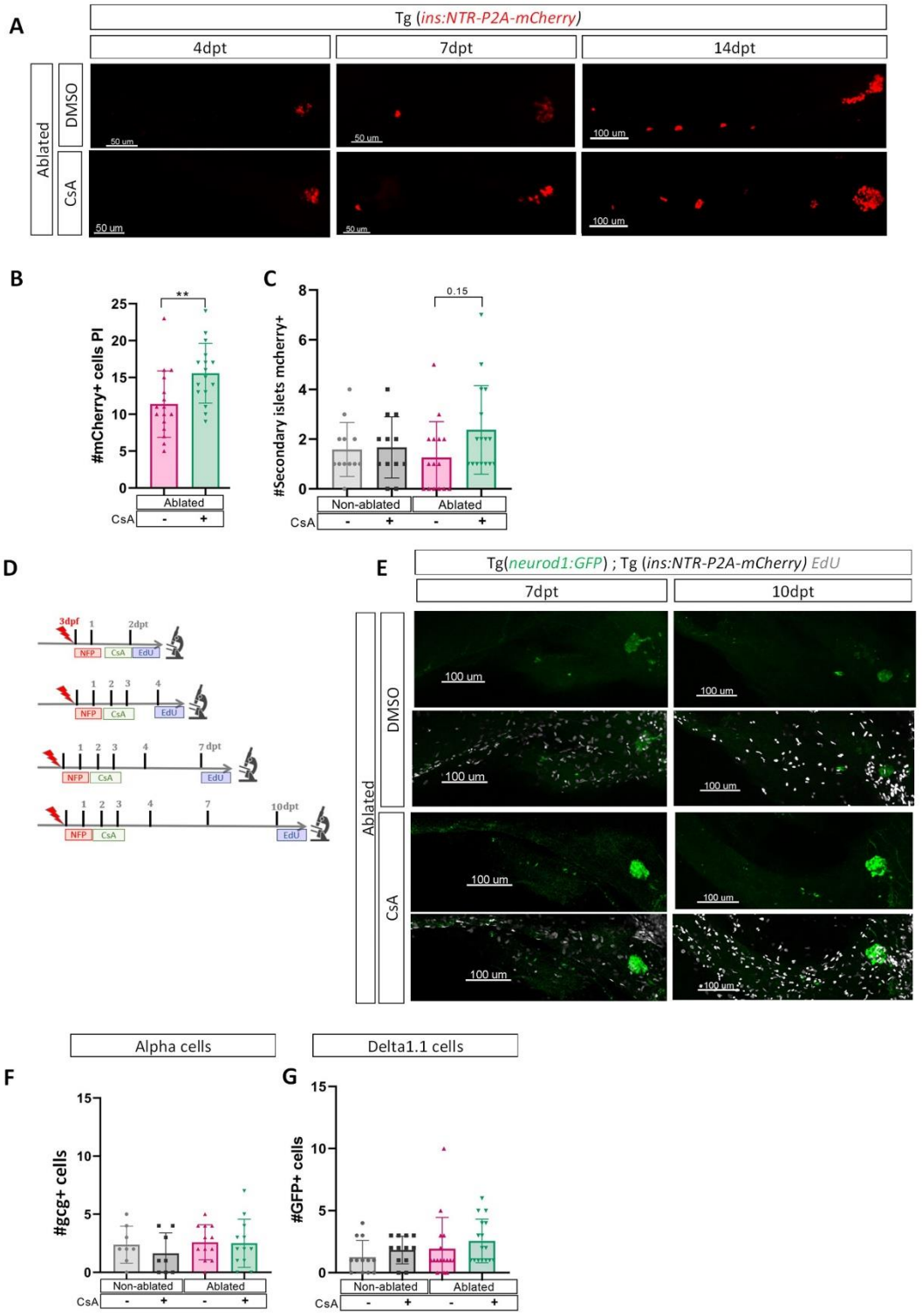

898

Figure 4 supplemental

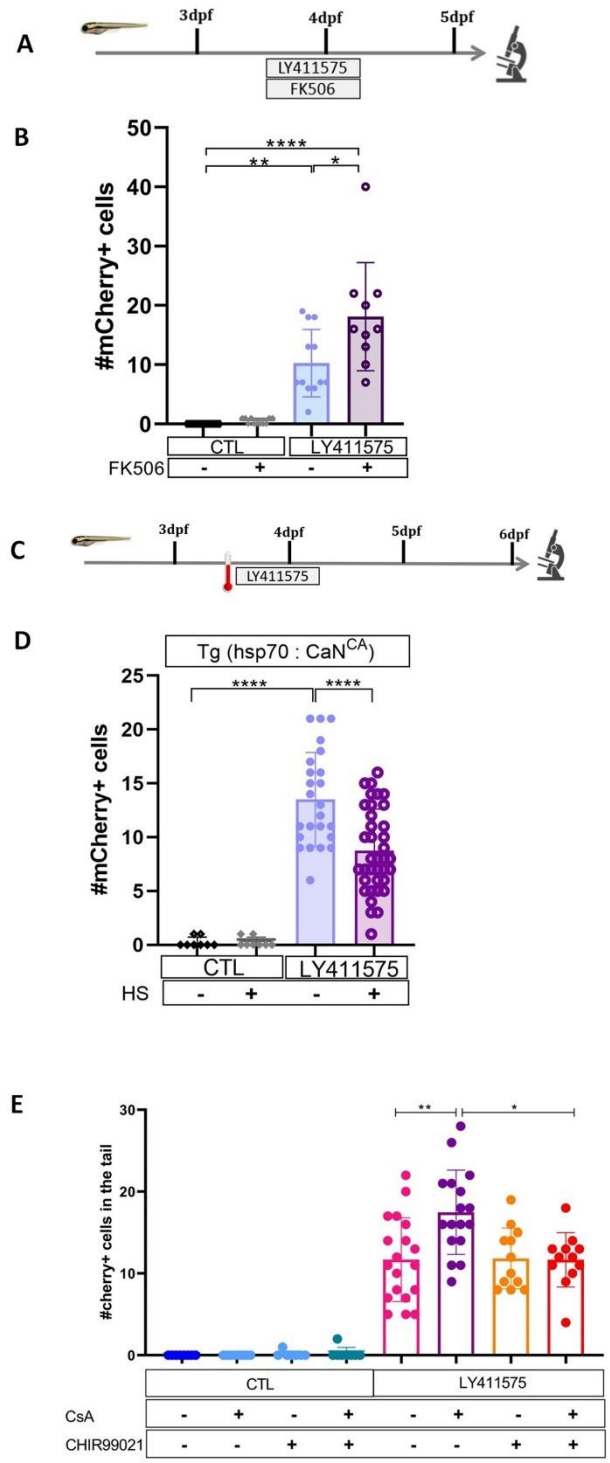

Figure 5 supplemental

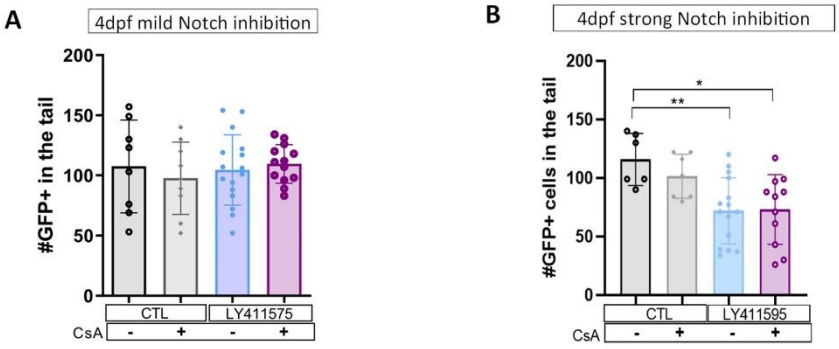

900

Figure 6 supplemental

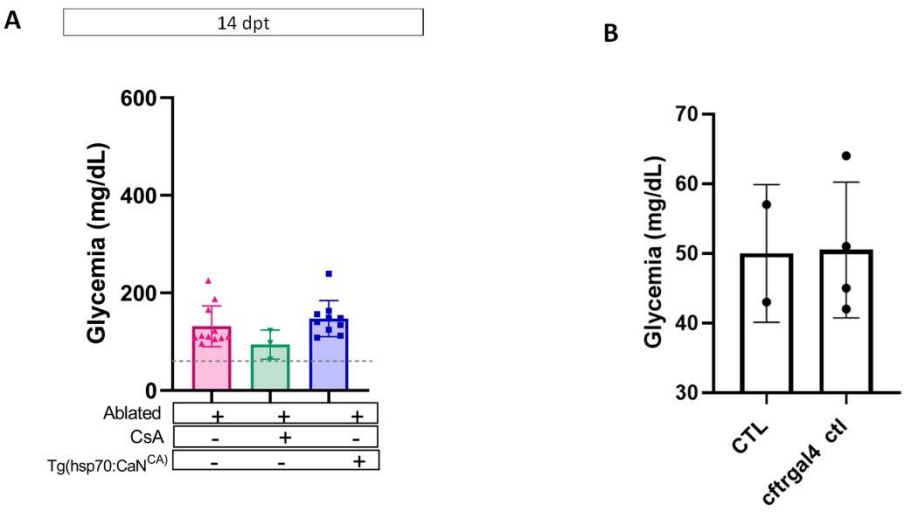

901